

Silica Fiber with Large and Thermodynamically Stable Second Order Optical Nonlinearity

Yan Yin

**Thesis submitted to the Faculty of the
Virginia Polytechnic Institute and State University
in partial fulfillment of the requirements for the degree of**

MASTER OF SCIENCE

in

Electrical Engineering

APPROVED:

Yong Xu, Chairman

Anbo Wang

Randy Heflin

April 24, 2008

Blacksburg, Virginia

**Key words: SHG efficiency, fiber tapering, ISAM CHISAM film, SHG
measurement, film surface improvement**

Copyright © 2008, Yan Yin

ALL RIGHT RESERVED

Silica Fiber with Large and Thermodynamically Stable Second Order Optical Nonlinearity

Yan Yin

**Yong Xu, Chairman
Electrical Engineering**

ABSTRACT

In this thesis, we demonstrate, theoretically, that, by depositing a regular fused-silica fiber with optical nonlinear molecules, strong and thermodynamically stable SHG can be obtained. Our experiments also provide strong evidence for the theory.

Start from the basic Maxwell equation, we derive the SHG efficiency that the excited power translates into the SHG signal. According to the SHG efficiency equation, a small radius and a long length will help to result in a high SHG efficiency, which also increases with the excited power. We fabricate silica fiber tapers with radius less than 5 μm through either wet etching or heating while stretching. Through improving the stretching setup, and adroitly manipulating both the stretching rate and the heating temperature, we are able to control the taper loss less than 1 dB. Then we dip taper part into cationic solution and anionic solution alternatively to have ISAM/CHISAM film on it. By improving the surface quality of film around a silica fiber taper, we are able to control film loss of PAH/PR film to less than 2 dB for 5 bilayers.

We set up a SHG measurement stage for a nonlinear fiber, and develop a measurement method during the experiments. We have shown that by depositing (PAH/PB)₁₀ films around a fiber taper with a diameter around 5 μm , we can obtain high SHG signal. The ratio of the obtained SHG signal to the excitation power for such a nonlinear fiber is more than 10 times of that of a 125 μm single mode fiber with the same length. Our experiment result provides strong evidence that centrosymmetric material can be used as SHG material.

Acknowledgements

There are many people I should acknowledge. First of all, I would like to express my deep gratitude to my advisor, Dr. Yong Xu, for bring me to his group and accepting me as one of your graduate research assistants. I would also like to thank him for showing such confidence in my abilities and encouraging me to perform to the best of my capabilities. Thank you for your professional guidance, advice, inspiration and continuous support technically and financially.

I am also deeply indebted to Dr. Anbo Wang for letting me work in Center for Photonics Technology. I benefit so much from his comment on my presentations and his advice academically and personally. Also thank to Dr. Randy Heflin for providing me his optical lab setup for the SHG measurement, and teaching me on ISAM films. Both Dr. Wang and Dr. Heflin are great committee members, and thank them for their time and valuable comments on my thesis.

A special thank goes to Dr. Ming Han for his inspiration and education on optics and experiment setup. Thanks so much to Dr. Kristie Lenahan Cooper, from whom I learned a lot about ESA films and its deposition procedures. Thanks to Cemil Durak for working together with me. Thank you for giving me so much information about ISAM/CHISAM films, and discussing problems with me. Thanks to Evan Lally for his advice and suggestion about my experiments as well as his important comments upon my thesis. Thanks to Yaoshun Jia for some importance advice on experiments.

I am grateful to Erika Gifford, kai cheng, Vaibhav Jain, Jason Ridley and Reza Montazami for their explanation when I got any question in Dr. Heflin's lab. I would also like to acknowledge Drothy Wang, Kathy Wang, Chen Ma, Jiajun Wang, Bo Dong and all staff and students at CPT for their assistance and friendship.

Personally, I would like to thank my parents, for their endless encouragement, love and support.

Table of Contents

chapter 1. Introduction.....	1
1.1 Introduction to Nonlinear Optics	1
1.2 Optical Nonlinearity of Nanoscale Self-Assembled Multilayer Films	3
1.2.1 Second-harmonic generation optical materials and technology.....	3
1.2.2 Introduction to Ionically Self-assembled Monolayers (ISAMs)	4
1.2.3 Covalent-Hybrid Ionically Self-Assembled Multilayer (CHISAM) Technique.....	6
1.3 Organization of the Thesis.....	7
chapter 2. Theoretical Analysis of the SHG Efficiency of the Silica Fiber with Nonlinear Film.....	9
2.1 Construction of Nonlinear Fiber.....	9
2.2 Derivation of the SHG Efficiency	10
2.2.1 Electrical Field of second harmonic mode	10
2.2.2 Effective Nonlinear Coefficient and further simplification	11
2.3 Estimation and Discussion	13
chapter 3. Sample Fabrication.....	16
3.1 Sample Structure.....	16
3.2 Fiber Tapering	16
3.2.1 Wet Etching of Optical Fiber	16
3.2.2 Stretching Optical Fiber Taper.....	20
3.3 ISAM / CHISAM Film Deposition	25
3.4 Process Automation	30
3.5 Work on Loss Reduction	31
3.5.1 Taper Loss and Film Loss of Early Samples.....	31
3.5.2 Process Optimization and Result of Loss Reduction	33
chapter 4. Experiment Setup and Data Analysis.....	39
4.1 Experiment Setup and Measure Method	39
4.2 Data Analysis.....	41
4.2.1 Early SHG measurement of fiber taper with (PAH/PR) ₅ film:	41

4.2.2 Measurement of a fiber taper coated with (PAH/PB)₁₀ film: 43

4.2.3 The Impact of High Power at Forepart of SMF28 43

chapter 5. Conclusion and Future Work 47

5.1 Conclusion 47

5.2 Future work 47

Reference 50

List of Illustrations

Figure 1-1: Process that ISAM/CHISAM film is built up	4
Figure 2-1: A second order nonlinear fiber, with a cylindrical silica core and layers of nonlinear molecules oriented along radial direction	9
Figure 3-1: Dip etch setup.....	17
Figure 3-2: Etching process of a single mode fiber.....	19
Figure 3-3: SEM image of etched silica fiber tip.....	20
Figure 3-4: Setup for heat-assisted deformation of optical fiber	21
Figure 3-5: Theory of CTS real-time monitoring of taper loss	22
Figure 3-6: Microscope photographs of sample No. 8 with a radius around 5 μm : 5 times magnification (left) and 50 times magnification (left).....	24
Figure 3-7: Optical power transmission loss through fiber taper, measured with OSA..	25
Figure 3-8: Different SHG signal under the same excitation of different films	28
Figure 3-9: Absorption of different films	29
Figure 3-10: SEM image of PAH/PR ISAM films on silica fiber.....	30
Figure 3-11: The spectrum of the fiber path before the sample is spliced into it. (see Figure 3-7(a)) The light source is the 850 LED	31
Figure 3-12: Loss caused by taper-stretching and film-deposition for sample 8. Here, the x-axis denotes the measure time (twice per layer, see table 3-2 for detail.)	32
Figure 3-13: Comparison of two samples using different fabrication methods: (a) a traditional method; (b) the new method we developed during our research	35
Figure 3-14: Loss of the samples that fabricated with improved film-deposition technique	36
Figure 3-15: Total loss of sample 10.....	37
Figure 3-16: Analysis of the loss caused by film deposition for sample 10.....	38

Figure 4-1: Figure 4-1: Setup for SHG measurement of nonlinear fiber sample..... 39

Figure 4-2: Measurement step 2 and 3 41

Figure 4-3: Early measurement of bare single mode fiber and fiber taper with nonlinear film..... 42

Figure 4-4: Compare of ratios of SHG to reference signal of the sample 48 and a single mode fiber with same length 43

Figure 4-5: Experiments to explore the SHG comes out of the forepart of the fiber with high excitation power 44

Figure 5-1: Experiments to explore the SHG comes out of the forepart of the fiber 48

List of Tables

Table 3-1: Description of Materials used for ISAM/CHISAM films	26
Table 3-2: Detail description of the parameters of solutions	26
Table 3-3: Loss increase with film layers for sample 8	33
Table 4-1: SHG of a SMF28 without loss and with high loss	45
Table 4-2: SHG of sample 48 Vs SHG of looped SMF 28	45

chapter 1. Introduction

Second-harmonic generation (SHG) is the phenomenon that an input wave generates another wave with twice the optical frequency in SHG materials. This phenomenon has many applications in nonlinear optics, surface characterization and biomedical imaging.

Currently, most SHG materials used in optical devices are bulky crystals, which are both expensive and hard to fabricate. It is also difficult to incorporate bulky components into the fiber optical systems. The SHG fiber we proposed here, however, is quick and easy to fabricate as well as inexpensive. The appearance of SHG fibers will definitely make the optical devices cheaper and more compact.

In the last two decades, there have been extensive investigation of silica fibers in the field of nonlinear optics field¹. Since second order nonlinearity requires non-centrosymmetry, nonlinear effects of silica fibers are limited to third order susceptibility due to the centrosymmetry of silica fibers. Second order nonlinearity in silica fibers can be generated by breaking centrosymmetry of the silica glass using different poling techniques, such as optical, electrical and UV poling^{2,3,4,5,6,7,8,9}. There are significant drawbacks associated with these methods. For example, the second order susceptibility of the poled fiber is weak and thermodynamically unstable, which can disappear in a few months.

In this thesis, we demonstrate, theoretically, that, by depositing a regular fused-silica fiber with optical nonlinear molecules, strong and thermodynamically stable SHG can be obtained. Our experiments provide strong evidence for this theoretical prediction.

1.1 Introduction to Nonlinear Optics

Electromagnetic radiation is described by Maxwell's equation as follows:

$$\nabla \times \vec{E} = -M_i - \frac{\partial \vec{B}}{\partial t} \quad (0.1)$$

$$\nabla \times \vec{H} = \vec{J}_i + \vec{J}_c + \frac{\partial \vec{D}}{\partial t} \quad (0.2)$$

$$\nabla \cdot \vec{D} = \rho_{ev} \quad (0.3)$$

$$\nabla \cdot \vec{B} = \rho_{mv} \quad (0.4)$$

The definitions and units of the quantities are:

\vec{E} = electric field intensity (volts/meter)

\vec{H} = magnetic field intensity (amperes/meter)

\vec{D} = electric flux density (coulombs/square meter)

\vec{B} = magnetic flux density (webers/square meter)

\vec{J}_i = source electric current density (amperes/square meter)

\vec{J}_c = conduction electric current density (amperes/square meter)

\vec{M}_i = source magnetic current density (volts/square meter)

ρ_{ev} = electric charge density (coulombs/cubic meter)

ρ_{mv} = magnetic charge density (webers/cubic meter)

In dielectric material, the electric flux density is related to the electric field density by

$$\vec{D} = \epsilon_0 \vec{E} + \vec{P} \quad (0.5)$$

where \vec{P} is the net electric polarization generated by bound charge within the material in response to the applied electric field. Also, the electric polarization may be expressed by electric field intensity in the following form

$$P_i = \epsilon_0 \chi_{ij} E_j + 2d_{ijk} E_j E_k + 4\chi_{ijkl} E_j E_k E_l + \dots \quad (0.6)$$

where P_i is the i th component of the instantaneous polarization and E_i is the i th component of the instantaneous electric field intensity ($i, j, k, l = x, y, z$)¹⁰. Coefficients χ_{ij} , d_{ijk} and χ_{ijkl} represent for linear susceptibility, second-order and third-order nonlinear optical susceptibilities, respectively. In this thesis, we only consider the second-order nonlinearity $2d_{ijk} E_j E_k$, which is responsible for the SHG phenomenon.

1.2 Optical Nonlinearity of Nanoscale Self-Assembled Multilayer Films

1.2.1 Second-harmonic generation optical materials and technology

For second-harmonic generation, the standard requirement is that the nonlinear optical material must be noncentrosymmetric. Traditional optical fiber, which is centrosymmetric, cannot produce significant second harmonic responses. However, by depositing suitable SHG material around the centrosymmetric material with radial molecular orientation, the nonlinear fiber can produce significant SHG responses. The theoretical analysis about this structure is shown in Chapter 2, and we will discuss the suitable SHG materials here.

Besides the noncentrosymmetry, the material used for SHG must also satisfy:

1. Low absorption and low scattering loss at the interested wavelength and the second-order wavelength
2. Homogeneity and easy-processability
3. Optical, thermal, chemical and environmental stability
4. Easy applicability for Lab or industry integral system

Traditional second order nonlinear crystals such as lithium niobate, Potassium dihydrogen phosphate (KDP) and beta-barium borate (BBO) have been widely used in academic research and industrial applications. However, for fiber applications, a silica fiber based structure that possesses strong second order nonlinearity would be ideal. Such a fiber structure cannot be produced by using the standard nonlinear crystals. In addition, these crystals are expensive and not versatile enough to be applied everywhere. Thus, people developed organic films to fulfill their demand for cheap, thin and versatile NLO materials.

Several novel methods including, Electric-field poled polymers^{11,12,13}, Langmuir-Blodgett (LB) films^{14,15}, and covalent self-assembled monolayer structures^{16,17}, have been reported to generate nonzero even-order nonlinear optical susceptibilities. Among these techniques, ionically self-assembled monolayer (ISAM) technique is considered to be much simpler and less expensive with long-term stability susceptibilities. In this thesis, I

will deposit the ISAM/CHISAM films on a single mode fiber (SMF) taper to generate second harmonic responses.

1.2.2 Introduction to Ionically Self-assembled Monolayers (ISAMs)

Self-assembly techniques were first developed in 1980s, as an alternative to LB films¹⁸ and the early applications were based mainly on silane-SiO₂¹⁹ and metal phosphonate chemistry²⁰. Furthermore, the electrostatic attraction between oppositely charged molecules provides driving forces for the formation of multilayers which yields better positioning of individual layers, independent of the nature, size and topology of the substrate. G. Decher and co-workers first developed a technique for the construction of multicomposite films with ionic attraction in 1991.^{21,22,23} The polymeric thin films fabricated monolayer by monolayer by immersing the substrate into oppositely-charged solutions (also called polyanion and polycation solutions) alternatively, referred to here as ionically self-assembled monolayers (ISAMs). Figure 1-1 shows the process of fabricating Ionically Self-assembled Monolayers (ISAM) / covalent-hybrid ionically self-assembled multilayer (CHISAM) film. A glass slide is immersed into cationic solution and anionic solution alternatively to have ISAM/CHISAM film on it

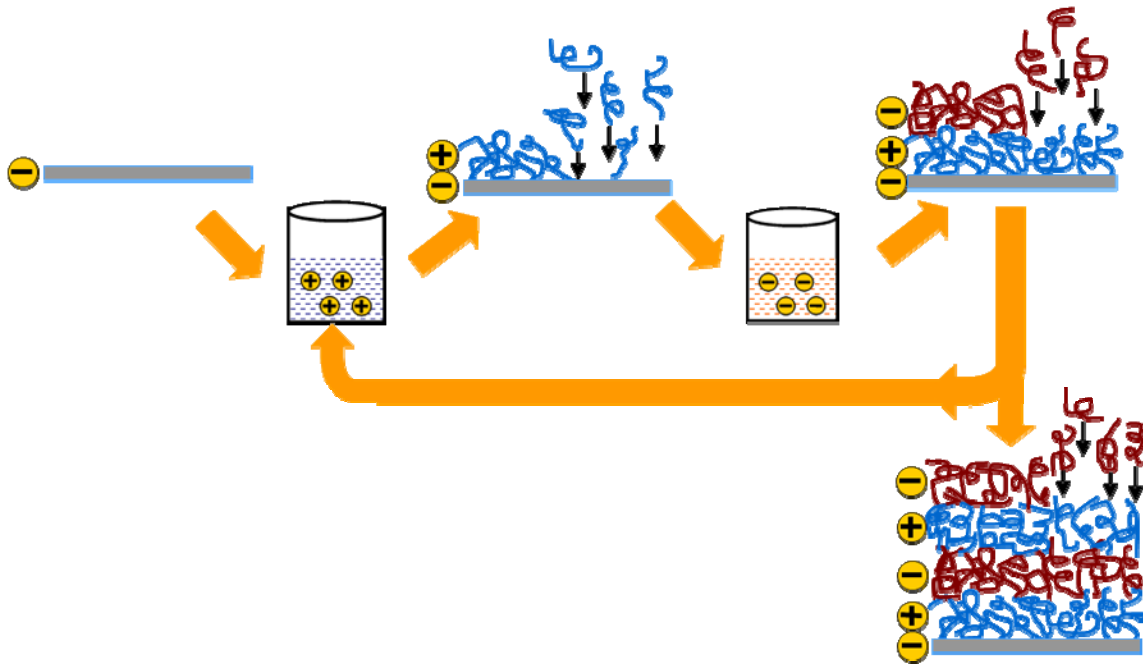


Figure 1-1: Process that ISAM/CHISAM film is built up

Compared with other self-assembly techniques, ISAM technique is simple and inexpensive with long-term stability and is thus extensively employed. The core of the layer-by-layer assembly technology is the repulsion of equally charged molecules for restriction to a single layer and the attraction of oppositely charged molecules for absorption of another layer on top of the first one. Thus, the fabrication of the film just involves immersing the substrate alternatively into oppositely-charged solutions. Since the adsorption is determined by the electrostatic attraction of the cationic layers and the anionic layers, each layer is self-limiting in thickness, which is normally 0.3 to 20 nm per layer. The properties of the ISAM film also include:

Stability

The use of polyelectrolytes rather than small molecules is due to the good adhesion of the former to give high stability to the films. The use of polymers with high charges but low ionic strength as both anionic and cationic polyelectrolytes is necessary and rinsing before switching to the other polymer solution can remove loosely attached polymer molecules. (The rinsing can also avoid contamination for the next adsorption solution with the former one.) Besides, small ions must be incorporated to compensate the excess charge and appropriate PH values should be adjusted for weak polyelectrolyte absorption.

J. R. Heflin and co-workers fabricated the nonlinear (NLO) ISAM films using dye Poly S-119, which consists of a “poly (vinyl amine backbone) with an ionic azo-dye chromophore, as polyanion and PAH (allylamine hydrochloride)” as polycation.²⁴ The nonlinear susceptibility generated by this film is found to be stable over nearly three years. Its susceptibility decreases by 20% as the temperature is raised to 150 degrees. Yet the second order susceptibility completely recovers to its origin value upon cooling, due to the reforming of these broken bonds. This thermal and temporal stability of polymer NLO films is very desirable for device applications.

Parameter-adjustability

Monolayer thickness and refractive index of ISAM films can be controlled precisely with solution parameters.^{24,25} At each PH value, film thickness and absorbance increase with the increased salt concentration. However, at each salt concentration, the thickness and absorbance decrease with the increased PH value. The increase of salt concentration and decrease of PH value strengthen the ionic strength, which allows more curvature and loops every layer. That leads to dramatic increases in bilayers thickness from less than 1 nm to a few nms. PH value and the salt concentration can also tune the bulk refractive index between the low and the high refractive index of the polyanion and the polycation by adjusting the percentage of the two polymers (Assume the two polymer have different refractive index). This precisely character-tuned property of ISAM is now used extensively in different sensor fabrications.

Typical adsorption times per layers are usually minutes for polyelectrolytes^{26,27} and hours for gold colloids^{28,29}, varying with molar masses, concentration, and agitation of solutions.

Homogenization and linearity

The film is macroscopic homogeneous due to the interpenetration of adjacent layers and avoids the defects in truly crystalline films. The homogeneity of the film also makes the film thickness linearity increase with the increase of the bilayers.³⁰ The density and the thickness of every bilayer does not change much³⁰, and the absorbance of the ISAM is strictly linearly dependent on the number of bilayers.²⁴ However, if the substrate charge densities are very small, linear deposition can only be obtained after the first few layers when the “multiplication of surface functionality” gets appeased.^{31,32,33,34,35}

Also, ISAM nonlinear optical film has the potential to be made for low-loss waveguides because of its excellent homogeneity, simplicity and low fabrication cost.

1.2.3 Covalent-Hybrid Ionically Self-Assembled Multilayer (CHISAM) Technique

The covalent-hybrid ionically self-assembled multilayer (CHISAM) technique is adopted, as an improvement of the ISAM technique, in order to generate a bigger second-order NLO coefficient. This technique, involving covalently attaching the monomer

chromophores to the film at only one of its ends and ionically attaching the subsequent cationic layers, improves polar ordering and can produce a large $\chi^{(2)}$. The substitution of the polymer chromophores with monomer ones reduces the competitive dipole orientation and the random chromophores orientation. We may also build the film structure where the monomer chromophores point out to the direction that the film thickness increases and normally to the interface between the cationic and anionic layers. The molecules that we use in the thesis are dye Procion Red MX-5B and Procion Brown MX-GRN, of which the films made generate larger SHG's than those of the ISAM films .

1.3 Organization of the Thesis

In this thesis, we demonstrate that we can break the rule that the centrosymmetric materials cannot be used for second-harmonic generation by observing SHG responses in a silica fiber with full rotational and inversion symmetry with respect to the fiber central axis.

As presented in the following paragraphs, this thesis is organized into five chapters.

Chapter 1: Introduction to nonlinear optics and nonlinear self-Assembled multilayer films. Since our work involves interdisciplinary cooperation, the introductory part covers the knowledge in many disciplines.

Chapter 2: Theoretical analysis of the SHG efficiency of the silica fiber with nonlinear film. In this part, we derive the SHG efficiency from the fundamental the Maxwell's equation and explain why we could break the centrosymmetric-forbidden rule and obtain SHG response in a silica optical fiber

Chapter 3: Sample fabrication. This chapter presents the detail fabrication process of the fiber sample, with emphasis on how we solve the difficulty that people have never met and fabricate the samples that may be used for practical tests.

Chapter 4: Experiment setup and measrument procedure. This chapter notes how we are able to measure the SHG signal out of nonlinear fiber and how we optimize the optical path as well as the measure steps.

Chapter 5: Conclusion and future work. This chapter summarizes the entire thesis and also suggests directions of future research that would allow us to obtain higher SHG's with different centrosymmetric materials.

chapter 2. Theoretical Analysis of the SHG Efficiency of the Silica Fiber with Nonlinear Film

2.1 Construction of Nonlinear Fiber

We coat cylindrical silica fiber taper with nonlinear molecules using CHISAM technology. This method provides two advantages. First, the nonlinear molecules are aligned predominantly along the radial direction, generating the nonlinear susceptibility as big as 14 pm/V, approximately half of the value of LiNbO_3 ³⁶. Second, the nonlinear optical susceptibility generated by the CHISAM technology is significantly much more stable³⁶ than that of other nonlinear techniques such as Electric-field poled polymer^{11,12,13}, Langmuir-Blodgett (LB) films^{14,15} and covalent self-assembled monolayer structures^{16,17}.

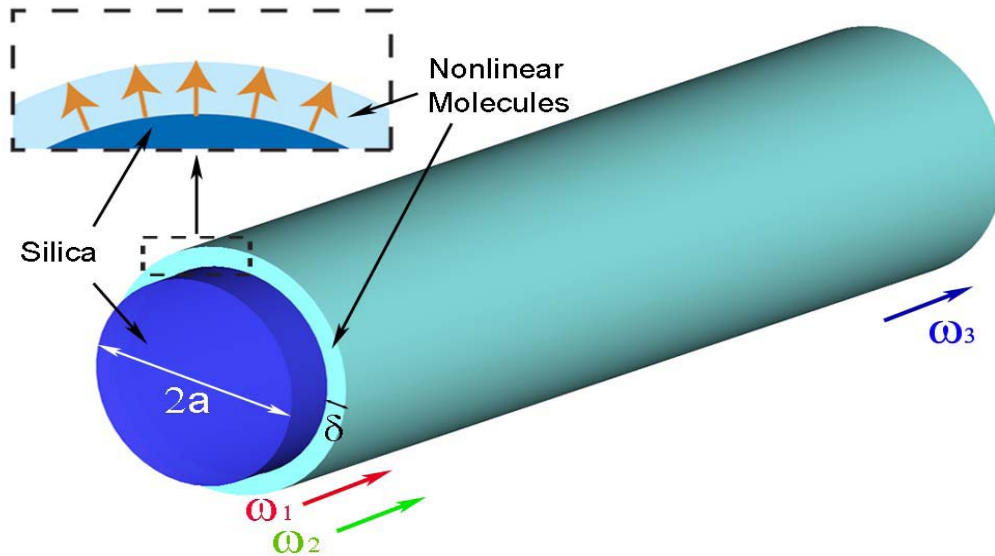


Figure 2-1: A second order nonlinear fiber, with a cylindrical silica core and layers of nonlinear molecules oriented along radial direction

2.2 Derivation of the SHG Efficiency

2.2.1 Electrical Field of second harmonic mode

Let's assume the nonlinear fiber is uniform along the direction of the wave propagation (i.e., the z axis) and the fiber supports three modes: two fundamental frequency modes $\vec{E}_{\omega_1}(\vec{r}, t)$ and $\vec{E}_{\omega_2}(\vec{r}, t)$ and a second harmonic mode $\vec{E}_{\omega_3}(\vec{r}, t)$. We may write them in the following form:

$$\vec{E}_{\omega_1}(\vec{r}, t) = \frac{1}{2} \left\{ E_{\omega_1}(z) \exp[i(\omega_1 t - \beta_1 z)] \vec{u}_{\omega_1}(\vec{r}) \right\} + c.c. \quad (2.1)$$

$$\vec{E}_{\omega_2}(\vec{r}, t) = \frac{1}{2} \left\{ E_{\omega_2}(z) \exp[i(\omega_2 t - \beta_2 z)] \vec{u}_{\omega_2}(\vec{r}) \right\} + c.c. \quad (2.2)$$

$$\vec{E}_{\omega_3}(\vec{r}, t) = \frac{1}{2} \left\{ E_{\omega_3}(z) \exp[i(\omega_3 t - \beta_3 z)] \vec{u}_{\omega_3}(\vec{r}) \right\} + c.c. \quad (2.3)$$

where E , β , $\vec{u}(\vec{r})$ are, respectively, the field amplitude, propagation constant and transverse field distribution at different frequencies ω_1 , ω_2 and ω_3 . Including the nonlinear polarization to the Maxwell equation (1.1-1.4) and equation (1.5), we have:

$$\nabla \times (\nabla \times \vec{E}) + \mu_0 \varepsilon \frac{\partial^2 \vec{E}}{\partial t^2} = -\mu_0 \frac{\partial^2 \vec{P}_{NL}}{\partial t^2} \quad (2.4)$$

The nonlinear polarization term \vec{P}_{NL} , the source of the second-harmonic mode, is given by

$$\vec{P}_{NL} = \frac{1}{2} \left\{ \tilde{d}^{(\omega_1 + \omega_2)}(\vec{r}) E_{\omega_1} E_{\omega_2} \exp[i(\omega_1 + \omega_2)t] \exp[-i(\beta_1 + \beta_2)z] \vec{u}_{\omega_1}(\vec{r}) \vec{u}_{\omega_2}(\vec{r}) \right\} + c.c. \quad (2.5)$$

where the tensor $\tilde{d}^{(\omega_1 + \omega_2)}(\vec{r})$ represents the second-order nonlinear coefficient of the dielectric medium¹⁰. Since we consider sum frequency generation, we assume

$$\omega_3 = \omega_1 + \omega_2 \quad (2.6)$$

Substituting Eq.(2.1-2.3) and Eq.(2.5-2.6) into Eq.(2.4), after straightforward derivations, we get:

$$\begin{aligned} & i \frac{dE_{\omega_3}}{dz} [-2\beta_3 \{ \hat{e}_z \times [\hat{e}_z \times \vec{u}_{\omega_3}(\vec{r})] \} - i \{ \hat{e}_z \times [\nabla_t \times \vec{u}_{\omega_3}(\vec{r})] + \nabla_t \times [\hat{e}_z \times \vec{u}_{\omega_3}(\vec{r})] \}] \\ & = \mu_0 \omega_3^2 \{ \tilde{d}^{\omega_3}(\vec{r}) E_{\omega_1} E_{\omega_2} \exp(-i(\Delta\beta)z) \vec{u}_{\omega_1}(\vec{r}) \vec{u}_{\omega_2}(\vec{r}) \} \end{aligned} \quad (2.7)$$

where, we use $\nabla = \hat{e}_z \frac{\partial}{\partial z} + \nabla_t$, $\Delta\beta = \beta_1 + \beta_2 - \beta_3$ and assuming $E_{\omega_3}(z)$ to be a slowly varying function in the propagation direction. After further derivation, we may write (2.7) as follows:

$$i \frac{dE_{\omega_3}}{dz} 2\omega_3 \varepsilon_0 \mu_0 v_g^{\omega_3} = \mu_0 \omega_3^2 E_1 E_2 \exp(-i\Delta\beta z) \iint_S d^2 r \bar{u}_{\omega_3}^*(\vec{r}) \tilde{d}^{\omega_3}(\vec{r}) \bar{u}_{\omega_1}(\vec{r}) \bar{u}_{\omega_2}(\vec{r}) \quad (2.8)$$

where, $v_g^{\omega_3}$ is group velocity at ω_3 frequency. Integrating nonlinear electrical field in the length of the fiber L and using the identity below, we obtain:

$$E_3 = -\frac{i\omega_3}{2\varepsilon_0 v_g^{\omega_3}} E_1 E_2 L e^{-i\frac{\Delta\beta}{2}L} \frac{\sin(\frac{\Delta\beta}{2}L)}{\frac{\Delta\beta}{2}L} \iint_S \bar{u}_{\omega_3}^* \tilde{d}_{\omega_3} \bar{u}_{\omega_1} \bar{u}_{\omega_2} d^2 r \quad (2.9)$$

2.2.2 Effective Nonlinear Coefficient and further simplification

If we assume that $E_1 = E_2$ and $\omega_3 = 2\omega_1 = 2\omega_2 = 2\omega$, and define a new scalar as effective nonlinear coefficient below:

$$D_{eff} = \left| \iint_S \bar{u}_{\omega_3}^* \tilde{d}_{\omega_3} \bar{u}_{\omega_1} \bar{u}_{\omega_2} d^2 r \right| \quad (2.10)$$

Substituting (2.10) into Eq.(2.9), we obtain:

$$|E_3|^2 = \frac{\omega^2}{\varepsilon_0^2 v_{2\omega,g}^2} |E_1|^4 L^2 \left[\frac{\sin(\frac{\Delta\beta}{2}L)}{\frac{\Delta\beta}{2}L} \right]^2 D_{eff}^2 \quad (2.11)$$

Since the nonlinear effect only exists in the nonlinear film, which surrounds the cladding of the fiber tightly, (see figure 2-1) the integration in (2.10) can be implemented only in the ring area, where the radial field components get the value at the edge of the fiber and $\tilde{d}_{\omega_3} \approx d_{zzz}$ is assumed (most of the nonlinear molecules are aligned along the direction that the nonlinear film grows, the r direction). Also, we assume $|\bar{u}_{\omega_1}^r(a)| = |\bar{u}_{\omega_2}^r(a)|$, and the effective nonlinear coefficient can be simplified to be:

$$D_{eff} = \pi a \delta \left| \vec{u}_{\omega_3}^r(a) \right| d_{zzz} \left| \vec{u}_{\omega_1}^r(a) \right|^2 = \pi a \delta \left| \vec{u}_{2\omega}^r(a) \right| d_{zzz} \left| \vec{u}_{\omega}^r(a) \right|^2 \quad (2.12)$$

where, a is the radius of the fiber and δ is the film thickness, which is in the order of tens of nanometers and significantly smaller than a .

Making use of the the orthonormalization of $\vec{u}_{\omega_3}(\vec{r})$:

$$\iint_S \vec{u}_{\omega_3}^*(\vec{r}) \cdot \vec{u}_{\omega_3}(\vec{r}) \epsilon_r(\vec{r}) d^2r = 1 \quad (2.13)$$

, we can have the energy of the nonlinear mode that flows through a section of fiber during the time Δt as:

$$\Delta \mathcal{E}(J) = v_{\omega_3, g} \Delta t \cdot \frac{|E_{\omega_3}(z)|^2}{2} \epsilon_0 \quad (2.14)$$

Since the optical power of the beam, $P_{\omega_3} (J/s)$ is the energy of the second-harmonic wave that flows through this section per second, we also have $P_{\omega_3} = \frac{1}{2} \epsilon_0 v_{\omega_3, g} |E_{\omega_3}(z)|^2$,

which also leads to

$$|E_{\omega_3}(z)|^2 = \frac{2P_{\omega_3}}{\epsilon_0 v_{\omega_3, g}} \quad (2.15)$$

Similarly, we can also obtain:

$$|E_{\omega}(z)|^2 = \frac{2P_{\omega}}{\epsilon_0 v_{\omega, g}} \quad (2.16)$$

Substituting the two equations into Eq.(2.11), we have:

$$\frac{2P_{2\omega}}{\epsilon_0 v_{2\omega, g}} = \frac{\omega^2}{\epsilon_0^2 v_{2\omega, g}^2} \frac{4P_{\omega}^2}{\epsilon_0^2 v_{\omega, g}^2} L^2 \left[\frac{\sin(\frac{\Delta\beta}{2} L)}{\frac{\Delta\beta}{2} L} \right]^2 D_{eff}^2 \quad (2.17)$$

Thus, we get the SHG efficiency as:

$$\eta_{SHG} = \frac{P_{2\omega}}{P_{\omega}} = P_{\omega} \frac{2\omega^2}{\epsilon_0^3 v_{2\omega, g} v_{\omega, g}^2} L^2 \left[\frac{\sin(\frac{\Delta\beta}{2} L)}{\frac{\Delta\beta}{2} L} \right]^2 D_{eff}^2 \quad (2.18)$$

where, $D_{eff} = \pi a \delta \left| \vec{u}_{2\omega}^r(a) \right| d_{zzz} \left| \vec{u}_{\omega}^r(a) \right|^2$.

In the case of phase matching¹⁰, where $\Delta\beta = \beta_{\omega_1} + \beta_{\omega_2} - \beta_{\omega_3} = 0$ Eq.(2.18) becomes:

$$\eta_{SHG} = \frac{P_{2\omega}}{P_{\omega}} = P_{\omega} \frac{2\omega^2}{\epsilon_0^3 v_{2\omega,g} v_{\omega,g}^2} L^2 D_{eff}^2 \quad (2.19)$$

which accounts for the most efficient second harmonic generation. For further simplification, we take $v_{2\omega,g} = v_{\omega,g} = c/\sqrt{\epsilon_r}$ and approximately

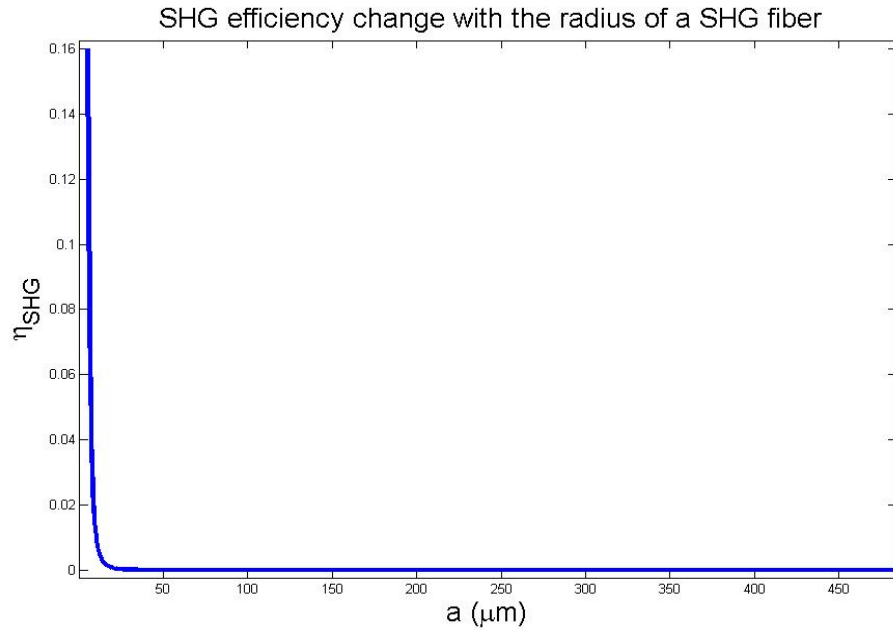
obtain $|\vec{u}_{2\omega}^r(a)| = |\vec{u}_{\omega}^r(a)| = \frac{1}{\sqrt{\pi a^2 \epsilon_r}}$ by estimating the integral Eq.(2.24) as

$|\vec{u}_{\omega_3}^r(a)|^2 \epsilon_r \pi a^2 = 1$. Then we substitute these into Eq.(2.19) and get:

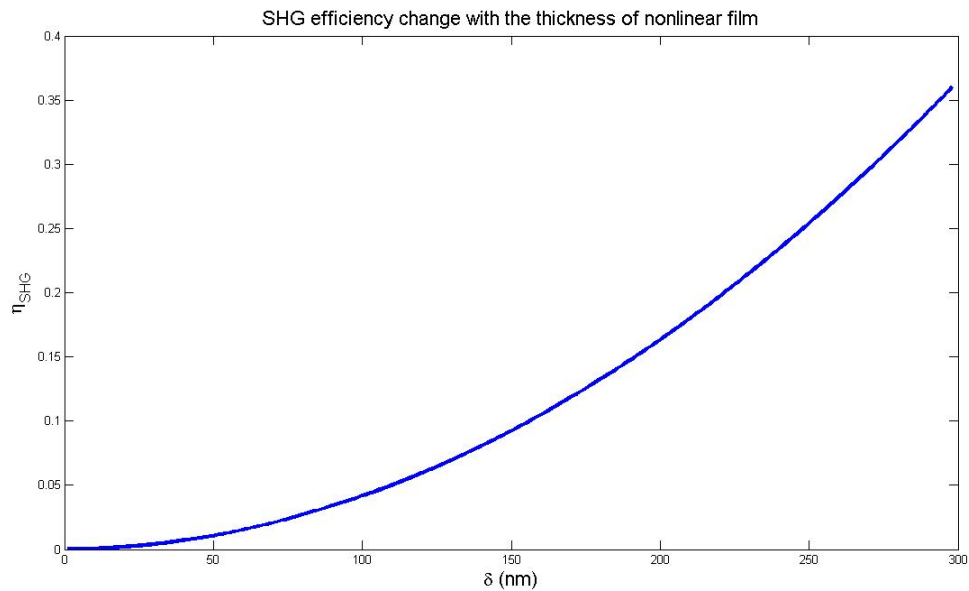
$$\eta_{SHG} = \frac{P_{2\omega}}{P_{\omega}} = 2\omega^2 \left(\frac{\mu_0}{\epsilon_r \epsilon_0} \right)^{3/2} \frac{P_{\omega}}{\pi a^2} \left| \frac{\delta}{a} d_{zzz} \right|^2 L^2 \quad (2.20)$$

2.3 Estimation and Discussion

We have developed the nonlinear efficiency in an optical fiber, and the simplified form under phase matching condition may be used to obtain a high second order nonlinearity using a silica-based optical fiber. According to (2.20), the nonlinear efficiency has quadratic dependence on increases with the reciprocal of the radius of a SHG fiber quarticly and the thickness of the nonlinear film quadricly, respectively. Figure 2-2 gives illustration that SHG efficiency increases if we decrease the radius of a SHG fiber and increase the thickness of nonlinear films.



(a) If we assume the other factors act as 100 in total, SHG efficiency decreases quartically as the radius of fiber increases from 0.5 mm to 5 μm .



(b) If we assume the other factors act as 10 in total, SHG efficiency increases quadratically as the thickness of nonlinear film increases from 3 nm to 300 nm.

Figure 2-2: SHG efficiency changes with fiber radius and film thickness

If we assume the film thickness is 50 nm and the value of d_{zzz} half of that of LiNbO₃, through a fiber with radius of 1 μm and length of 200 μm , a pump wavelength of 1 μm has SHG efficiency above 10%.

Here the unit of the nonlinear optical susceptibility, d_{zzz} , defined by $P = d_{zzz}E^2$ has the unit of $\frac{\text{s}^7\text{A}^3}{\text{m}^4\text{kg}^2}$. Another frequently used susceptibility $\chi_{rrr}^{(2)}$, is defined by $P = \epsilon_0\chi_{rrr}^{(2)}E^2$, and has the unit of $\frac{\text{pm}}{\text{V}}$. To convert the value between the two unit systems, we simply use: $\chi_{rrr}^{(2)} = d_{zzz} / \epsilon_0$.

From the analysis above, we find that we can potential achieve a large second order nonlinearity by reducing the fiber radius, using a longer fiber length, increasing the nonlinear film thickness, and satisfying phase matching condition. Thus, our aim is to deposit the nonlinear films as thick as possible on a section of fiber taper with a diameter less than 10 μm .

chapter 3. Sample Fabrication

3.1 Sample Structure

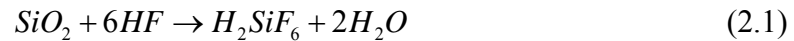
In this chapter, we discuss the experimental implementations of the SHG fiber which we have theoretically analyzed in chapter 2. First we get a taper silica fiber through either wet etching or simultaneous heating and stretching, because the nonlinear efficiency increases with the reciprocal of the radius of a fiber quarticly (see figure 2-2). The goal is to produce fiber taper with radius less than 5 μm . Next we deposit ISAM / CHISAM film around the taper part of the silicon fiber. Finally, we investigate the total loss due to the fiber taper and the nonlinear film deposition.

3.2 Fiber Tapering

We can get a taper silica fiber with a radius less than 5 μm through either wet etching or by simultaneously heating and stretching the silica fiber.

3.2.1 Wet Etching of Optical Fiber

Hydrofluoric Acid (HF) etching is one of the most commonly used technique for producing silica fiber tapers. The chemical principle can be described in the following equation:



For HF with a concentration from 47% to 49%, the etching rate of pure silica is around 1 μm per minute at room temperature isotropically. However, the etching rate depends significantly on the concentration of the HF acid and on the doping of the silica fiber. For example, the etching rate of the germania-doped core in the original HF liquid is about 11.5 times faster than that of the pure silica and 8 times faster than that of the fluorine-doped cladding³⁷. Furthermore, due to the consumption and evaporation of the HF molecules, the etching rate decreases faster than linearly with the reduction of the HF concentration. The variance of the etching rate gives us two tips when we carry out the wet etching of the silica fiber:

1. After the fiber core is exposed due to the etching, the etching rate becomes very fast. The observation interval decreases into the range of 1 minute.
2. After being used for etching for some time, the etching rate of the HF decreases and the etching time takes longer to complete the same goal.

Figure 3-1 illustrates how the fiber tip is etched in a fume hood. The buffer coating of the fiber is stripped over a section around 2 cm at one end. We cleave the fiber end to ensure a smooth and flat end facet. After the HF liquid with desired concentration is prepared in a plastic pipette, we plug the fiber into a plastic pipette with the striped end immersed within the HF liquid. Parafilm is used to fix the fiber in the pipette and to avoid the HF from evaporating out. Then, we put the pipette into a HF- resist beaker. The whole process is performed in the fume hood. The graduate transition caused by the dip etching will then give a low loss when the light is guided from the normal part into the taper part. Thus, it is necessary to slope the pipette to increase the section of fiber that exposed to the HF vapor which is right above the liquid level and dense enough to give an effective etching. The more the fiber slopes, the longer the transition part is.

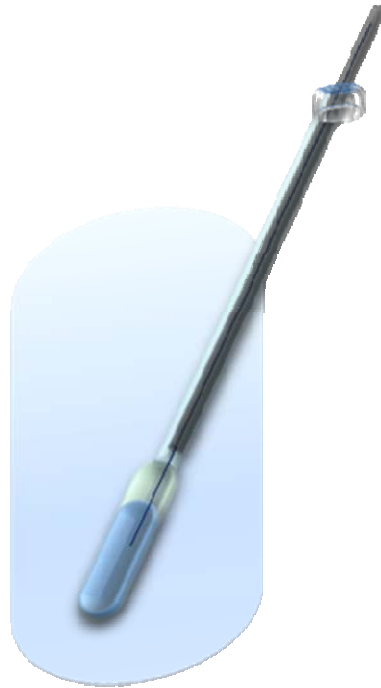
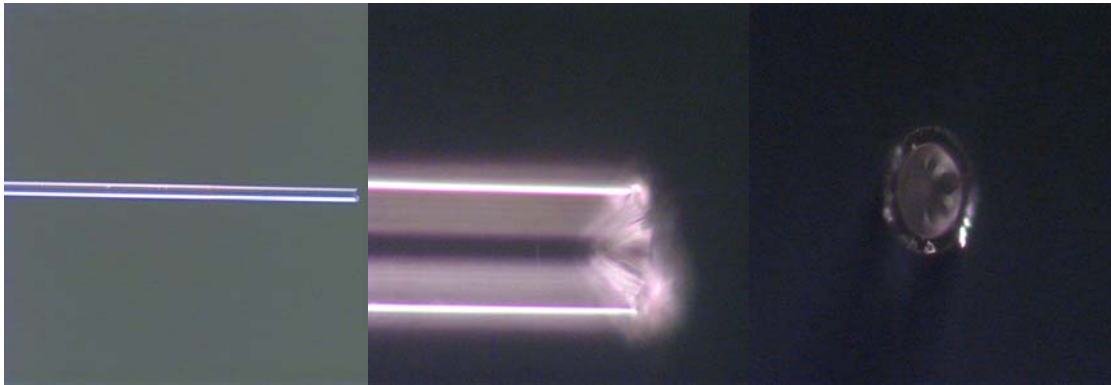


Figure 3-1: Dip etch setup

After the fiber is etched for an appropriate amount of time, we terminate the process by immersing the fiber tip into a plastic box full of water. After immersing the fiber in water for around 30 s, we move the taper fiber from fume hood, and then, rinse it under tap water. Figure 3-2(a) and (b) describes the etching process of a single mode fiber, which has a 9 μm germania-doped core and a 125 μm pure silica cladding. These figures are taken using the Zeiss Axiovert 25 Microscope.



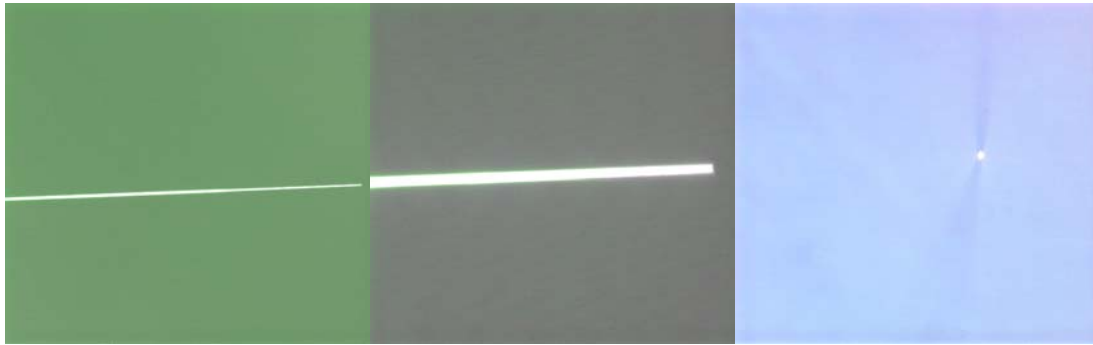
(a) After 40 min's etching in 47% HF (from left to right: 5 times magnification, 50 times magnification and 50 times magnification of the cutoff of the fiber tip, respectively), the fiber is around 55 μm in diameter.



(b) After being exposed to 13.3% HF for 20min, 30min and to 18.6% HF for 10 min the fiber is around 52 μm , 49 μm and 45 μm in diameter(50 times magnification of the cutoff of the fiber tip).



(c) After being exposed to 47% HF for a little while more (1 min to 5 min), the fiber got a smaller tip. (50 times magnification of the cutoff of the fiber tip)



(d) Finally, we have the fiber tip with a diameter less than $4\ \mu\text{m}$. (from left to right: 5 times magnification, 50 times magnification and 50 times magnification of the cutoff of the fiber tip, respectively)

Figure 3-2: Etching process of a single mode fiber

Figure 3-3 is a SEM image of a fiber taper that we fabricate through wet etching. The fiber taper is more than $300\ \mu\text{m}$ in length, with a radius of $3\ \mu\text{m}$.

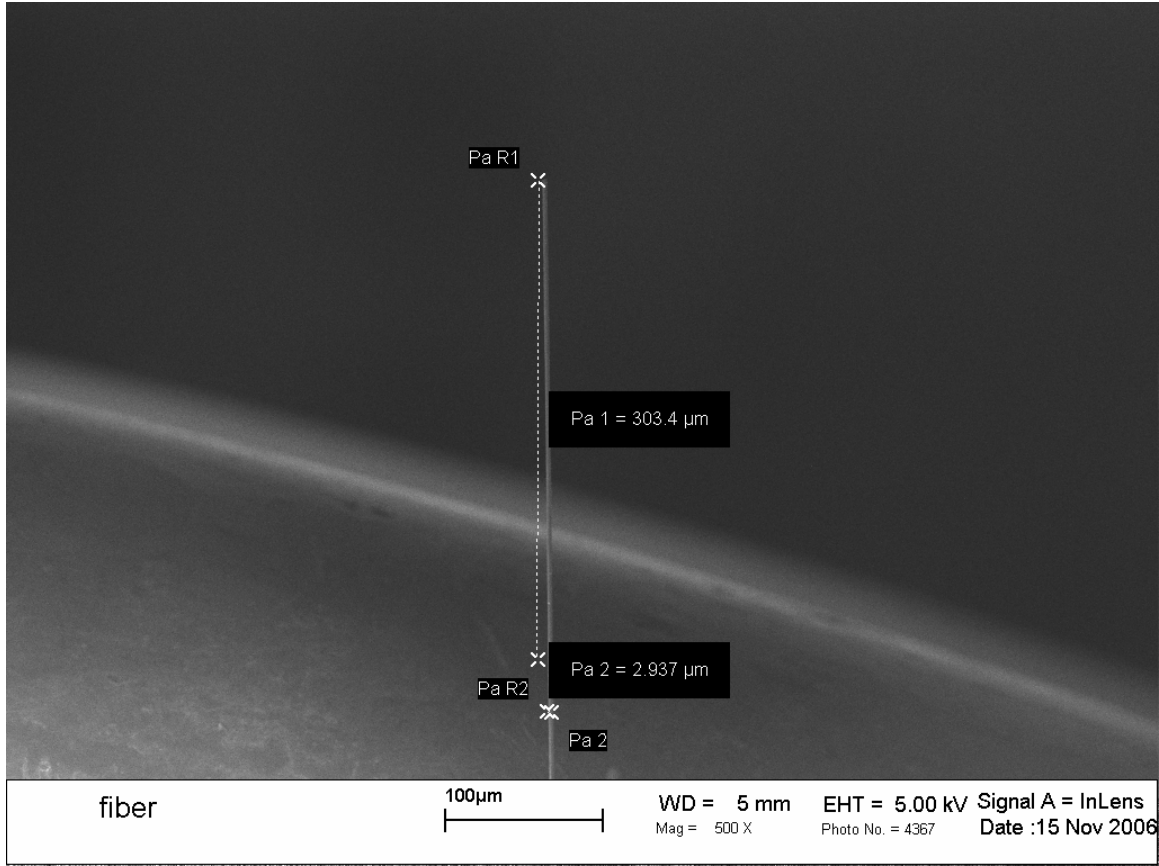


Figure 3-3: SEM image of etched silica fiber tip

3.2.2 Stretching Optical Fiber Taper

Although we are able to obtain a taper fiber with a small radius through wet etching in HF etchant, it is difficult to couple the light into or from the tip with diameter in the range of $1\ \mu\text{m}$. In an alternative approach, we use flame to heat the silica fiber close to the melting temperature and stretching the fiber to obtain a taper in the center of a single mode fiber. As a result, coupling light in or out of the fiber taper becomes much easier.

The key of this taper fabrication is to control extensional deformation rates so that extensional rates are the same everywhere³⁸. This helps to generate a gradual-transition taper shape, which generates a low loss when light transfers through the taper part.

The stretching setup shown in Figure3-4:

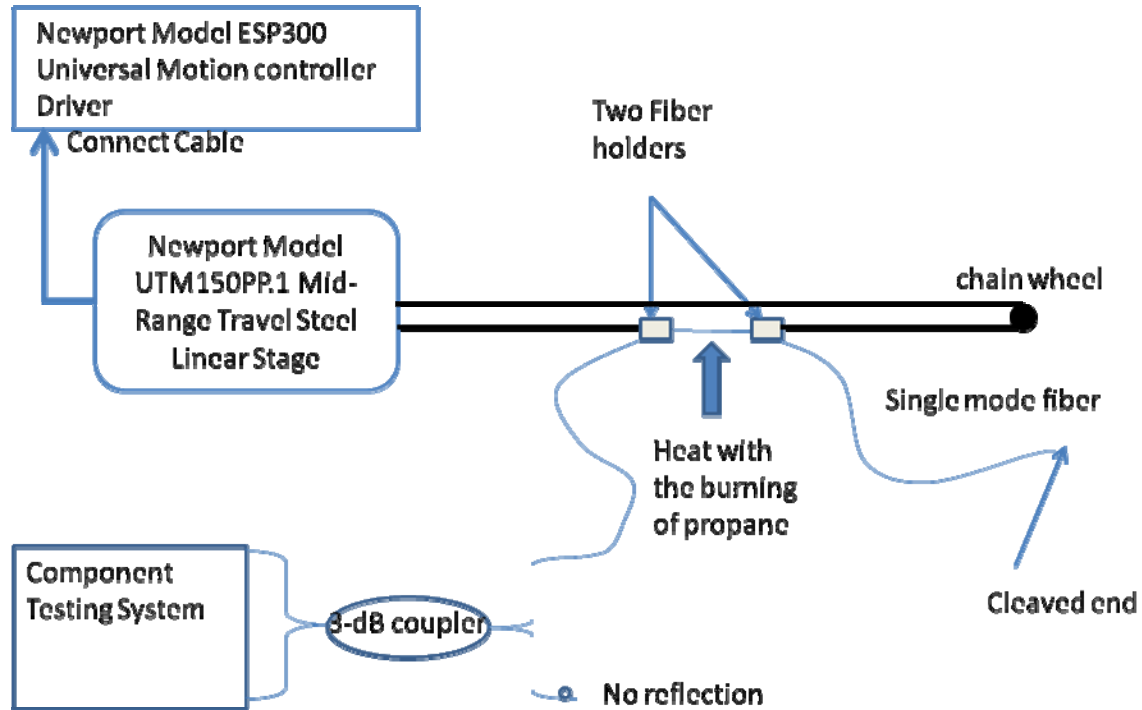


Figure 3-4: Setup for heat-assisted deformation of optical fiber

The fiber is clamped with two fiber holders which are connected to a motorized stage. The stage is connected to a Motion driver, which controls both the traveling direction and speed of the stage. Before stretching, we first light a nozzle of propane to generate enough heat that softens the silica fiber. Then, we set the speed of the travel stage through the motion controller at around 0.1mm/s to stretch the fiber into two directions. However, as the fiber gets thinner, the fiber is easily curled by the heating. In that case, we need either to increase the stretching speed or to decrease the heating temperature to make sure the taper part of the fiber is straight. In order to do so, one hand is used to control the distance between the flame and the fiber while the other one changes the stretching speed through the panel in the motion controller.

A component testing system (CTS) is used to monitor the taper process and give an estimation of the taper loss in time. It is a high resolution swept laser interrogator, which contains a fast swept laser, a high dynamic range detector and a real time operation system. Since the CTS continuously sweeps 5 times per second in the wavelength range

of 1520nm to 1570nm, it provides a real-time monitoring of the fiber stretching process. Figure 3-5 shows how CTS observes the taper loss during the stretching process.

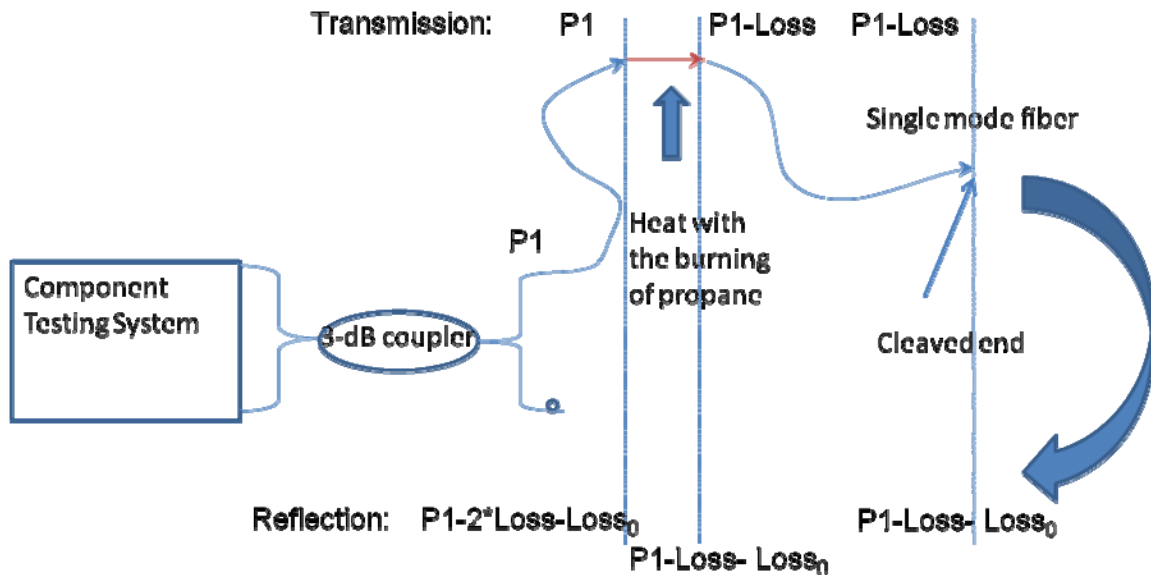


Figure 3-5: Theory of CTS real-time monitoring of taper loss

From figure 3-5, it is clear that, if the power of the light that launches to one end of the fiber is P_1 , after the light transmits through the taper part, the output power at the other end of the fiber is $(P_1 - \text{Loss})$, where the Loss is caused by the taper part. Since the other end of the fiber has been cleaved to be a flat surface, we assume the scattered power as Loss_0 and the reflected power of the light is still $(P_1 - \text{Loss} - \text{Loss}_0)$. Thus, according to figure 3-5, when the light ultimately reaches the detector of the CTS, the power is $(P_1 - 2 * \text{Loss} - \text{Loss}_0)$. If there is no taper in the fiber, the transmission loss of the fiber itself is very small and we would observe P_1 at the LCD screen of CTS. However, after the stretching begins, with the deformation process of the fiber, the taper loss increases. Thus, we would have the power shown on the LCD screen of CTS decreases to be P_2 . At that time, we estimate the taper loss to be $(P_1 - P_2) / 2$.

Another advantage of the real-time monitoring is that we may control the deformation by reading the power shown on the LCD screen. At the very beginning of the stretching, the power decreases very slowly. With the deformation of the fiber, there is a significant reduction of the power. In that case, we usually increase the stretching rate or move the flame farther from the original place to make sure the stretching part is

straight. If there is already an observable curl of the stretching part, that must be accompanied with a dramatic drop of power in the CTS screen. One method is developed to correct this situation. Move the flame around the curl point to avoid it from further curling. At the same time, we increase the stretching rate slowly and let the flame follow the curled point while keeping the flame from getting too close to it. By doing so, we would be able to see in the screen that the power gradually increases back. The interference pattern on the screen of CTS can be employed to judge the diameter of the taper part in order to decide whether the taper process should be stopped. After getting the fiber with desired diameter and taper loss, we need to transfer the taper fiber from the stretching setup to a slide.

In order to make fiber taper easy to be handled for film deposition and SHG measurement, we use a microscope slide as the substrate and apply the epoxy 907 gel (from miller-stephenson chemical co.) on the microscope slide, leaving around 2 cm apart, which is the rough length of the taper part. Then we put the slide on a three dimensional translation stage and glue toe fiber taper to the substrate using the epoxy. We keep a small distance of approximately 1-2 mm between the fiber taper and the microscope slide, which make the subsequent task of depositing the ISAM/CHISAM film easier.

In order to measure the diameter of the taper, we use the Zeiss Axiovert 25 Microscope to take a photograph of the taper part and then compare the photograph with the microscope image of another fiber with known diameter. The equation used to calculate the taper diameter is as follows:

$$\frac{d_1}{D_1} = \frac{d_2}{D_2} \quad (2.2)$$

D_1 and D_2 is what we measured in the photograph using a ruler while d_1 is the known diameter of the fiber. With equation 3.2, we are able to estimate the taper diameter d_2 . By comparing several groups of the estimating results with that measured in SEM, we find out the error is less than 10%. Right now, it is easy for us to fabricate the fiber taper with a diameter less than 5 micron. See figure 3-6 as an example:

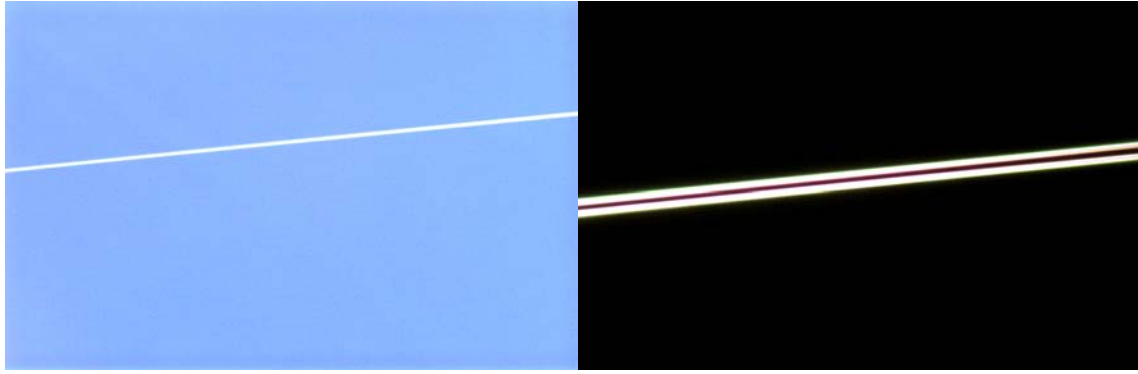
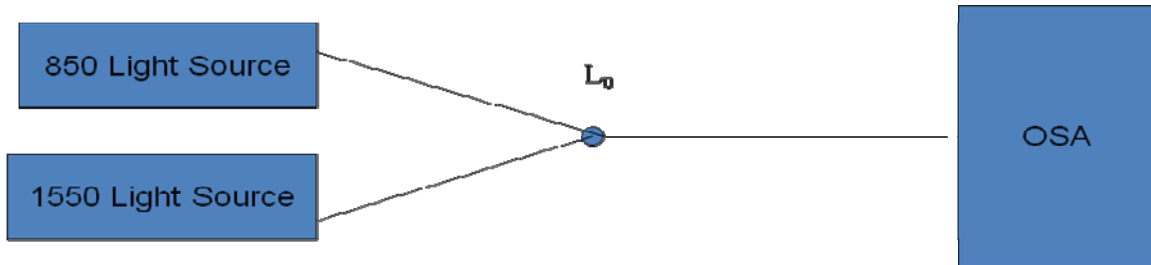
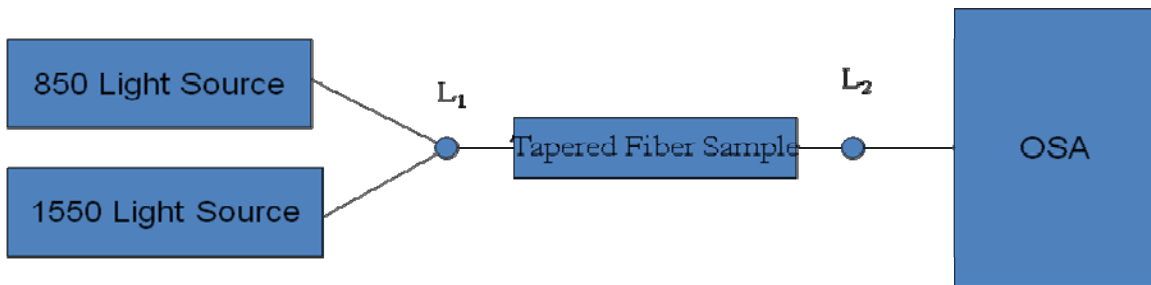


Figure 3-6: Microscope photographs of sample No. 8 with a radius around 5 μm: 5 times magnification (left) and 50 times magnification (left)

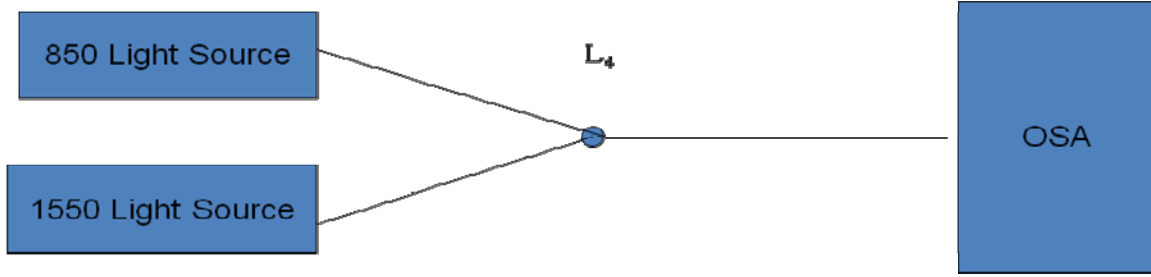
In order to measure of fiber taper loss more precisely, we use the procedure shown in figure 3-7 (a)-(d): The measurement process involves two LED light source (with emission wavelength at 850nm and 1550nm respectively) and the ANDO AQ-6315A Optical Spectrum Analyzer (OSA).



(a) Measure the optical path output in OSA (with no tapered fiber sample): Assume we get P1 and the loss caused by the splicing is L_0 ; the Output of the optical path with no connector is: $Loss1 = P1 - L_0$.



(b) Measure the output of the optical path with tapered fiber sample in OSA: Assume we get P2 and the loss of the splicing point is L_1 and L_2 ; We have the Output of the tapered fiber sample as: $Loss0 = P0 - L_1 - L_2$.



(c) Measure the optical path output in OSA (with no tapered fiber sample) again: Assume we get P3 and the Output of the optical path with no connector is: $Loss_2 = P_1 - L_4$. Note: $Loss_2$ normally is close while not equal to $Loss_1$ due to the instability of the Light Source and Optical Path.

Tapered Fiber Sample

(d) The estimated loss of the tapered fiber sample is: $Loss_s = Loss_0 - (Loss_1 + Loss_2) / 2$.

Figure 3-7: Optical power transmission loss through fiber taper, measured with OSA

3.3 ISAM / CHISAM Film Deposition

After we got a tapered silica fiber with the taper part fixed on a slide, we may deposit the ISAM/CHISAM film onto the taper part through alternatively dipping the slide into the cationic solution and anionic solution. The description of the cationic and anionic solutions that we used in the experiments is as noted in Table 3-1:

	Polycation Provider	Nonlinear Chromophores Provider (cationic solution)		
Name	PAH	PCBS	Procion Red	Procion Brown
Structure	poly(allylamine hydrochloride)	Poly{1-[4-(3-carboxy-4-hydroxyphenylazo)-benzenesulfonamido]-1,2-ethanediyl} Orange-yellow dye		

Molecular Weight	93 g/mol	369 g/mol	615 g/mol	767 g/mol
Obtained From	Sigma-Aldrich Chemical Company	Sigma-Aldrich Chemical Company	Sigma-Aldrich Chemical Company	Purification
storage life	Several months in refrigeratory	Several months in refrigeratory	6 – 7 hours	6 – 7 hours

Table 3-1: Description of Materials used for ISAM/CHISAM films

The polycation provider, PAH, is nonlinear inactive and only serves as an “adhesive”. The nonlinear chromophores provider, on the other hand, is anionic, and deposits on the PAH because of static force. The

The PH values, solution concentrations and the concentration of the salt also play important roles in the film’s character. In our experiments, we adjust these factors to generate the optimum SHG value.³⁹ The details of these factors are shown in table 3-2:

	Polycation Provider	Nonlinear Chromophores Provider (cationic solution)		
Name	PAH	PCBS	Procion Red (PR)	Procion Brown (PB)
concentration	10 mM/L	10 mM/L	5 g/L	5 g/L
PH value	7	7	10.5	10.5
Salt concentration	No salt	No salt	No salt	0.5 Mole/L
storage life	Several months in refrigeratory	Several months in refrigeratory	6 – 7 hours	6 – 7 hours

Table 3-2: Detail description of the parameters of solutions

Once the solutions are prepared, they need to be stirred for some time before it can be used to generate homogenous films. The stir time differs for different solutions. For PAH and PCBS, they need to be stirred overnight and around half an hour every time before they are used. For Procion red and Procion Brown, which cannot be kept more than 7 hours, the stir time is around half an hour. By including monomer chromophores to the film, the CHISAM films PAH/PR and PAH/PB can generate very strong second order nonlinear responses, with nonlinear susceptibility approaching the level of LiNbO_3 . In addition, by introducing NaCl into the nonlinear films, we can produce thicker films with larger nonlinear coefficients. We immerse slides into PAH and PR/PB solutions alternatively to have CHISAM films on that. Then we use Yag laser to generate 1064nm beams to incident on the slide. At the same time we also measure the SHG signal reflected from the slides with different rotation angels. The SHG signals under the same excited power of the films that we use are shown in figure 3-8:

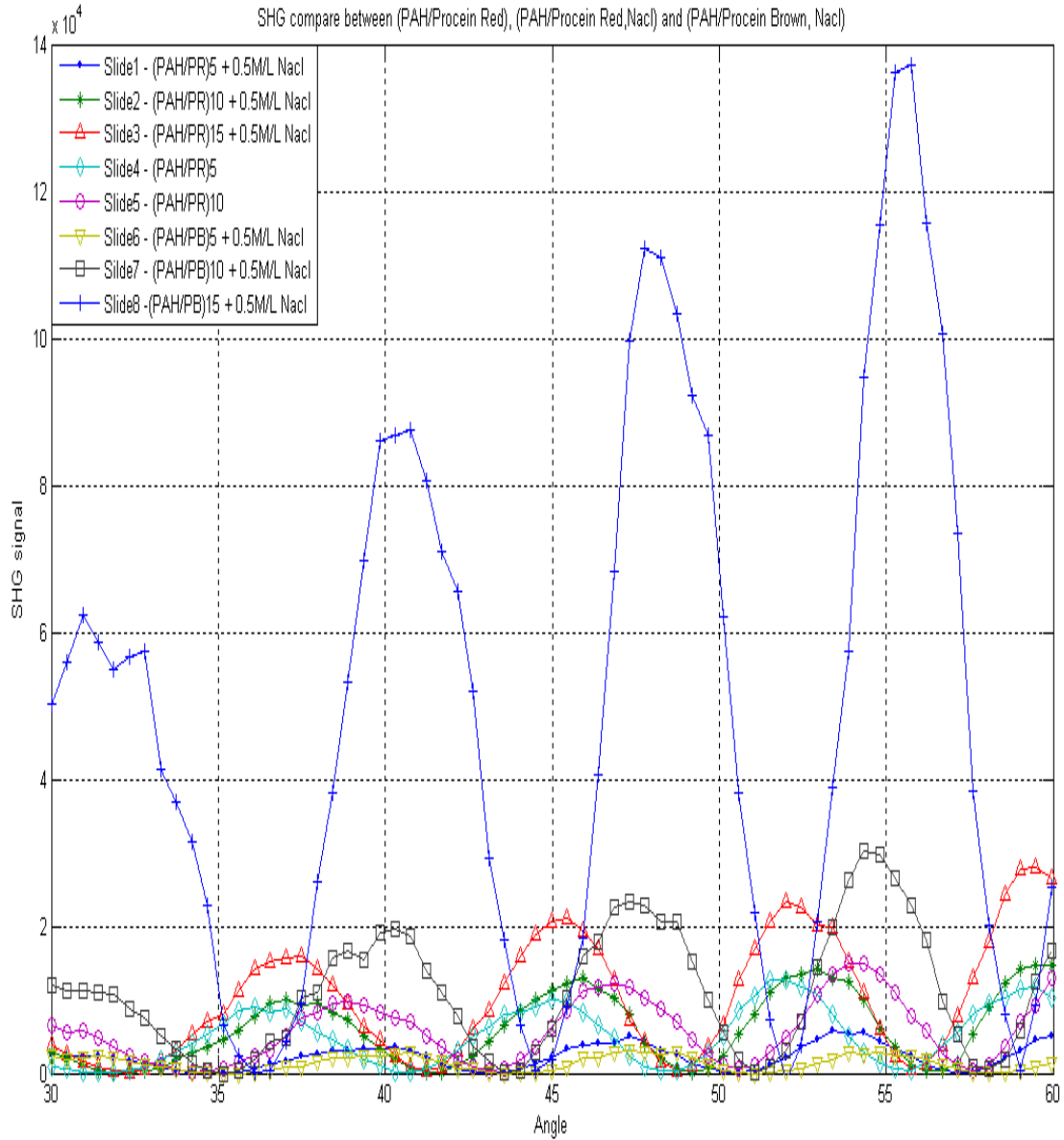


Figure 3-8: Different SHG signal under the same excitation of different films

The absorption in Figure 3-9 corresponds to the thickness of the films. We may refer to the absorption plotting to characterize the films that we have had on the fiber.

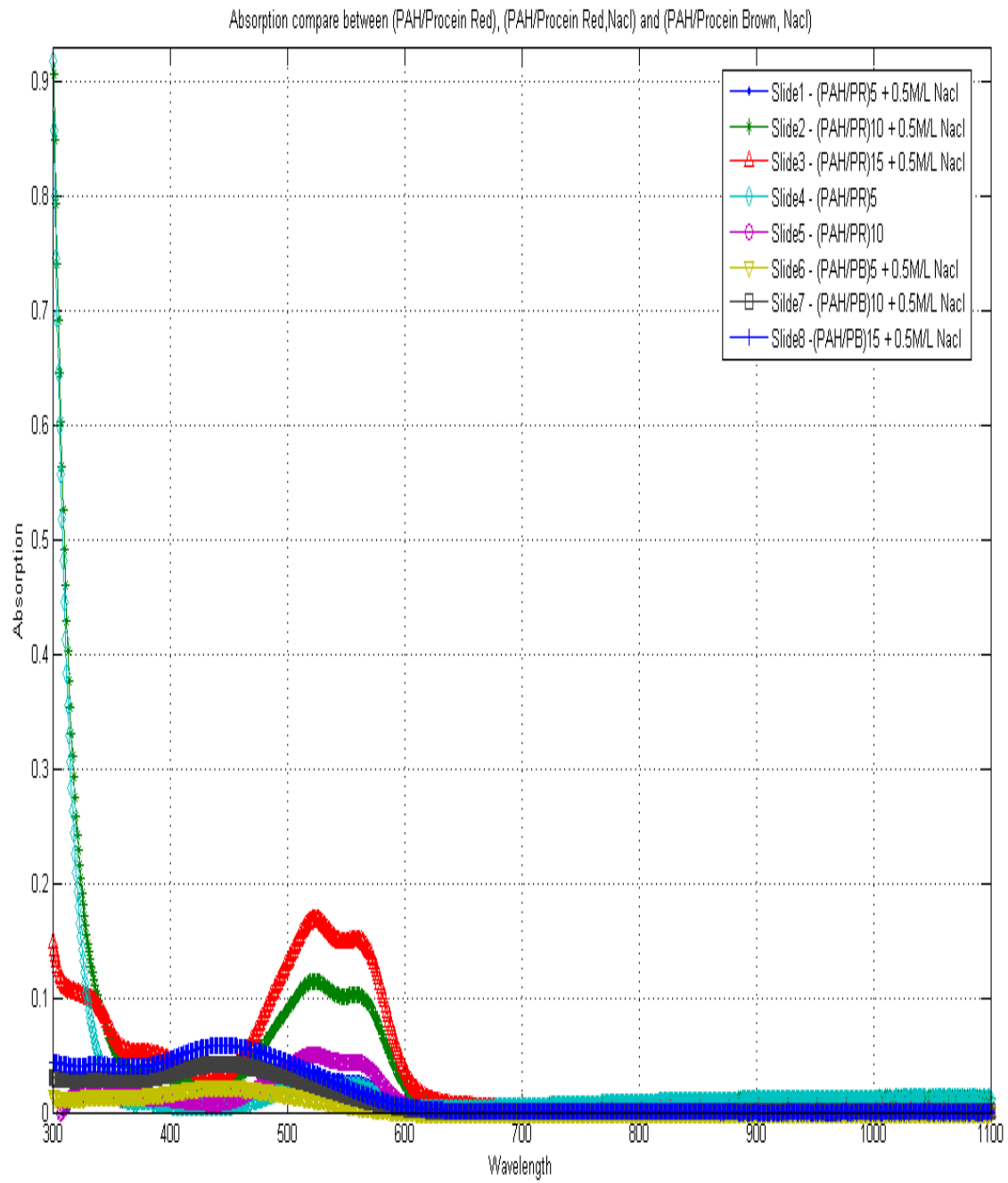


Figure 3-9: Absorption of different films

Figure 3-10 gives a SEM image which shows that CHISAM film is deposited on the surface of silica fiber.

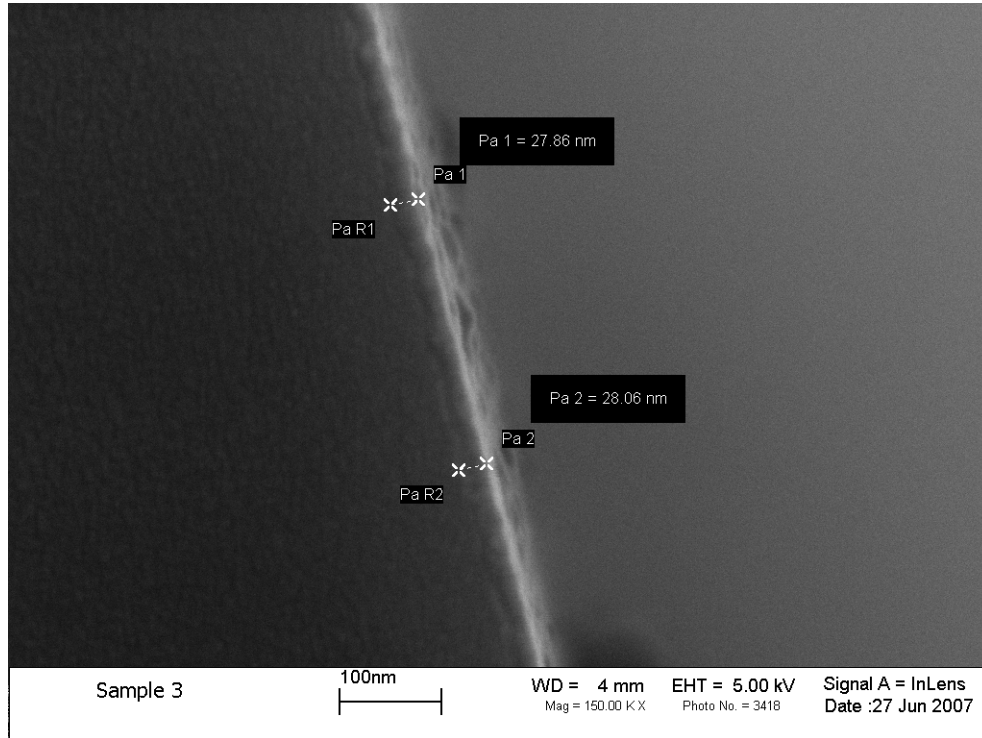


Figure 3-10: SEM image of PAH/PR ISAM films on silica fiber

3.4 Process Automation

The ISAM/CHISAM film depositions in this thesis were all fabricated using hand dipping methods unless specified otherwise. Automation of the ISAM process will allow high-speed synthesis of identical films on multiple substrates, which leads to significant saving in time and labor. For manufacturing purposes, the advantage of such automation is obvious - higher throughput and lower costs. The processing of the ISAM films can be automated using a Programmable Slide Stainer from the Richard-Allan Scientific Company.

However, the automatic deposition approach may lead to inhomogeneity across the film surface, which is even more significant when we deposit nonlinear film on a fiber taper with a diameter less than 10 μm . There are several reasons for the inhomogeneity. More will be discussed in section 3.5.2.

3.5 Work on Loss Reduction

After covering the taper section of the fiber taper with ISAM/CHISAM film, we need to characterize the loss of the nonlinear fiber. The loss measurement procedure taper has already been shown in Figure 3-7. If we denote the total loss of the sample as $Loss_t$, the loss due to the nonlinear film can be written as:

$$Loss_{Film} = Loss_t - Loss_s \quad (2.3)$$

We can observe the loss caused by the nonlinear film during the deposition process by performing a real time loss measurement. We write Matlab codes to read the data generated with the OSA, which gives the spectrum figures as shown in Figure 3-11.

3.5.1 Taper Loss and Film Loss of Early Samples

Figure 3-12 and table 2-2 gives a description of the film loss that increases with the number of film layers:

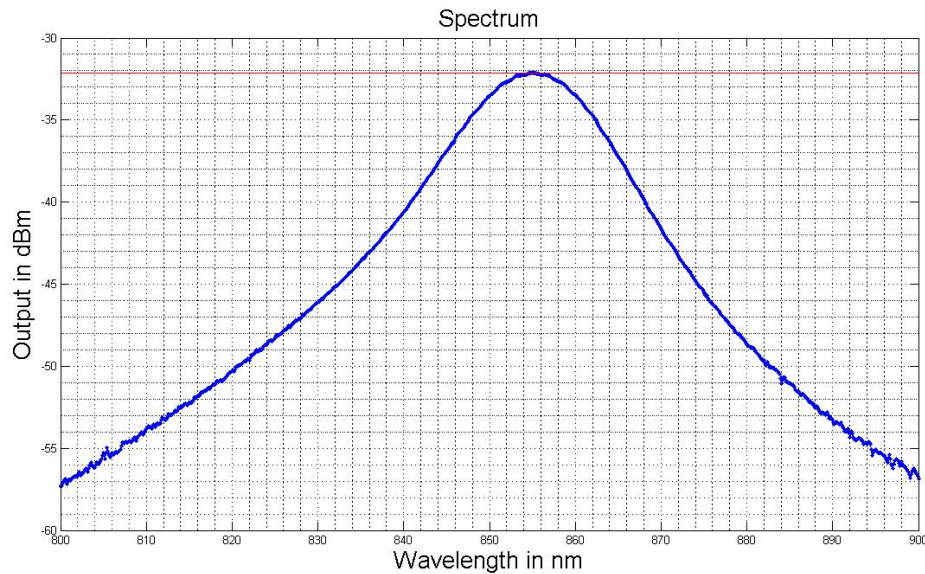


Figure 3-11: The spectrum of the fiber path before the sample is spliced into it. (see Figure 3-7(a)) The light source is the 850 LED

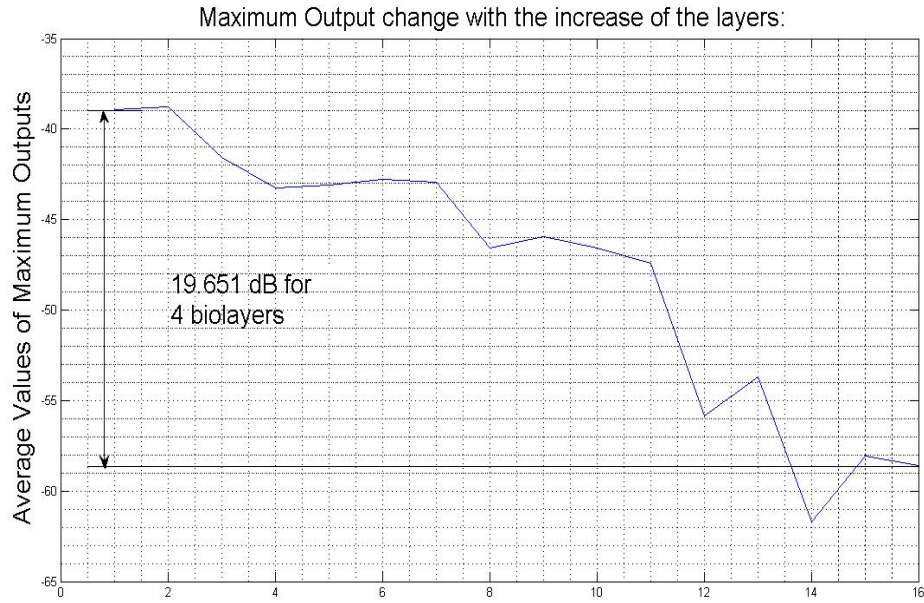


Figure 3-12: Loss caused by taper-stretching and film-deposition for sample 8. Here, the x-axis denotes the measure time (twice per layer, see table 3-2 for detail.)

Setting of OSA:

CTRWL: 850.000000; SPAN: 100.000000; REFL: -39.100000; LSCL: 5.000000
 RESLN: 5.000000; AVG: 1.000000; SMPL: 501.000000; SENS: "NR_HLD"; NMSK:
 "OFF"

Before grow film: 855.600 -39.096 85800				
	PAH	Water	Procion Red	Water
Peak wavelength(nm)	853.200000	854.000000	857.800000	850.400000
Peak power (dBm)	-38.939000	-38.778000	-41.544000	-43.254000
Measure time	1	2	3	4
Peak wavelength(nm)	850.400000	853.600000	856.600000	850.600000
Peak power (dBm)	-43.113000	-42.752000	-42.953000	-46.554000
Measure time	5	6	7	8

Peak wavelength(nm)	851.800000	855.200000	855.700000	855.800000
Peak power (dBm)	-45.960000	-46.565000	-47.433000	-55.869000
Measure time	9	10	11	12
Peak wavelength(nm)	855.000000	No signal	857.200000	No signal available
Peak power (dBm)	-53.705000	available	-61.704000	
Measure time	13		14	
Sip up the water: 857.000000 -58.058000 85815 (Measure time 15)				
Dry in the air for two hours: 856.600000 -58.590000 85816 (Measure time 16)				

Table 3-3: Loss increase with film layers for sample 8

According to figure 3-11, figure 3-12 and table 3-3, the loss caused by taper-stretching is 7 dB and the loss caused by 4-bilayer film is 19.651 dB. The total loss is 26 dB! Sample 8 gives relatively lower loss than other samples. For many samples, light signal cannot even be observed after transmit through them with just three bilayers, indicating losses bigger than 26 dB.

The high loss is not good for the SHG measurement, since second harmonic signal strength is proportional to the square of the pump power. In a high loss sample, the pump power decay dramatically, resulting in low second harmonic signal strength. Therefore, it is critical to reduce the nonlinear fiber sample loss to the range of a few dBs.

3.5.2 Process Optimization and Result of Loss Reduction

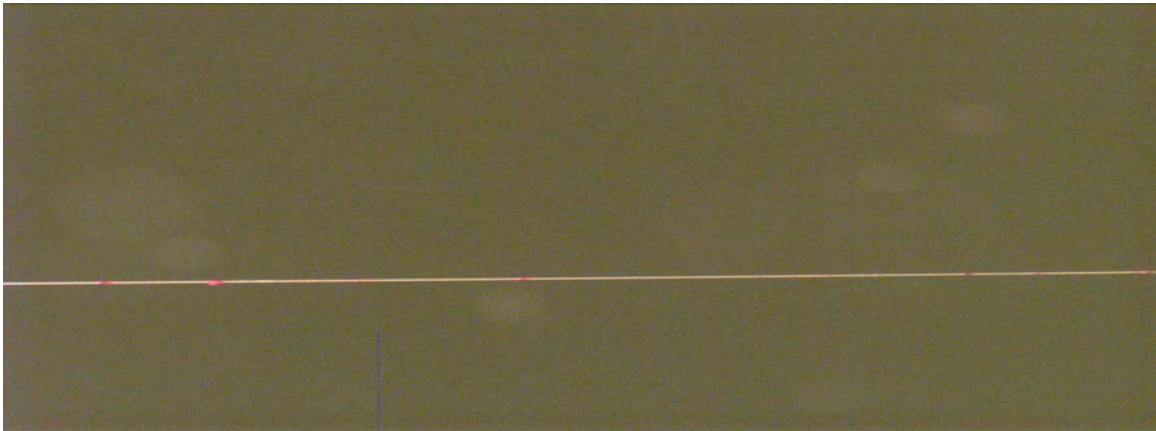
The taper-stretching loss has been reduced to less than 1 dB by controlling of both the stretching rate and the heating temperature. However, to reduce the loss caused by the film deposition is a hard job. The fiber loss due to nonlinear film is directly determined by the film surface quality. A coarse surface will create significant scattering and result in a big loss. In order to decrease this kind of loss, we need primarily to increase the film quality. The difficulty of this job lies in:

1. The ISAM/CHISAM film often has some surface coarseness in the range of 100 nm to 1 μm , even though other conditions are optimized.

2. In most situations, the film is deposited on a microscope slide, which tends to give a solid substrate that the molecules stretch out on the boundary. Here, we are using fiber with a diameter less than 10 μm which is not a stable substrate to generate compact film.

3. A method appropriate for one type film may possibly not work for another film.

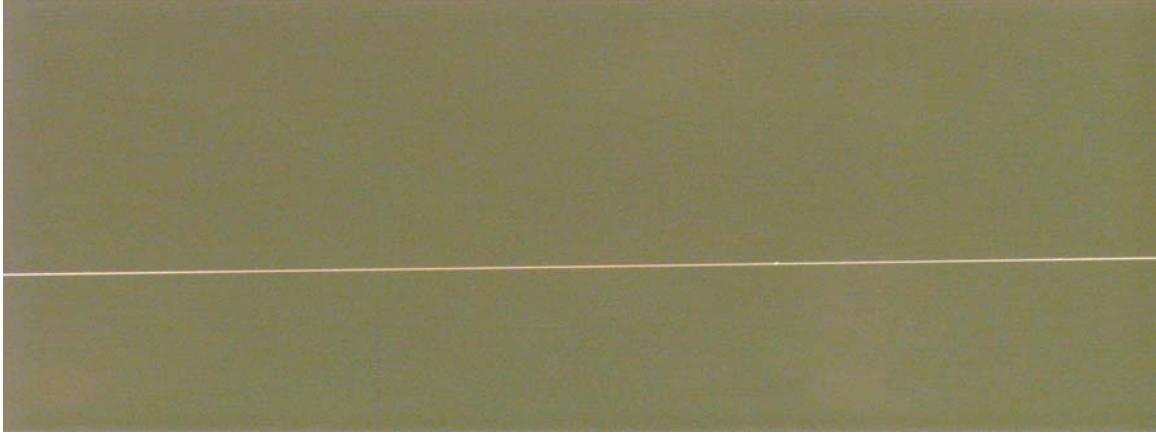
After half-year intense work, we tried tens of depositions conditions and has successfully reduced most of the film loss of PAH/PR film to less than 2 dB for 5 bilayers. Figure 3-13 gives the microscopic photographs of two samples that use different fabrication technologies. Both films are 5-bilayer PAH/Procion Red. Sample 27 which fabricated with a traditional method has a much bigger loss than sample 24 that fabricated with the technique that we developed⁴⁰.



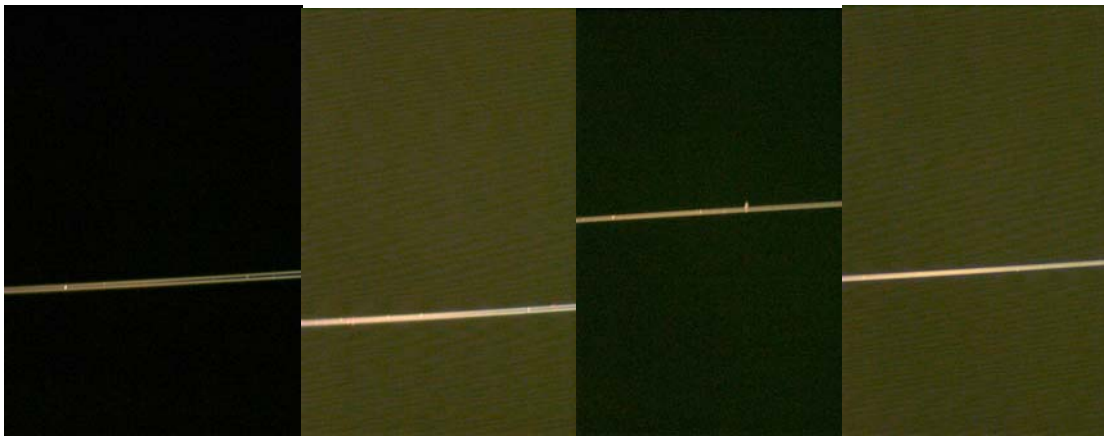
(a-1) 5 magnification of Sample 27



(a-2) 20 magnification of Sample 27



(b-1) 5 magnification of sample 24



(b-2) 20 magnification of Sample 24

Figure 3-13: Comparison of two samples using different fabrication methods: (a) a traditional method; (b) the new method we developed during our research

In figure 3-14, we provide the loss data for the samples that we fabricated using the improved film technique. The x-axis gives the sample number while the y axis represents the film loss. All the samples are $(\text{PAH/PR})_5$ with other parameters fixed. It is clear that most of the samples have a film loss that less than 2 dB.

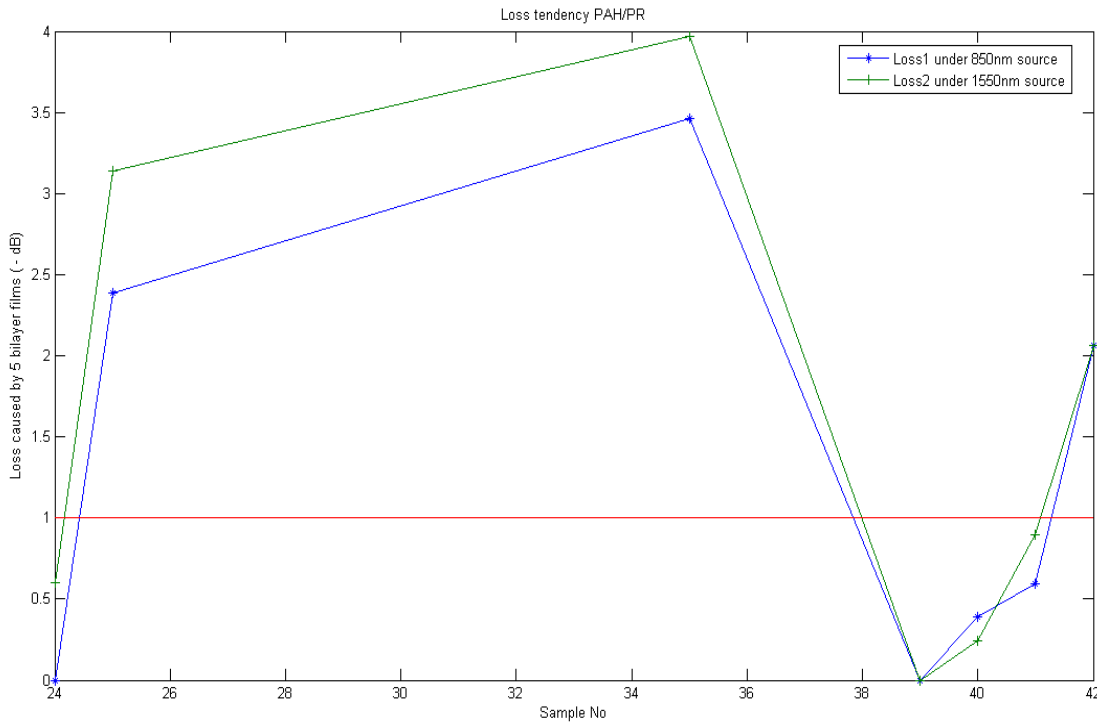


Figure 3-14: Loss of the samples that fabricated with improved film-deposition technique

Figure 3-15 described the total loss of sample 10, where I deposit (PAH/PR)₁₀ film on a fiber taper with a radius less than 10 μm. The total loss is measured by Dr. Liu’s group in PSU with a super continue light source. The y axis gives the transmitted optical power through the taper, while the x axis is the wavelength of the power. In this figure, we can see that the total loss of this sample is less than 5 dB at most wavelengths in the range from 700 nm to 1300 nm.

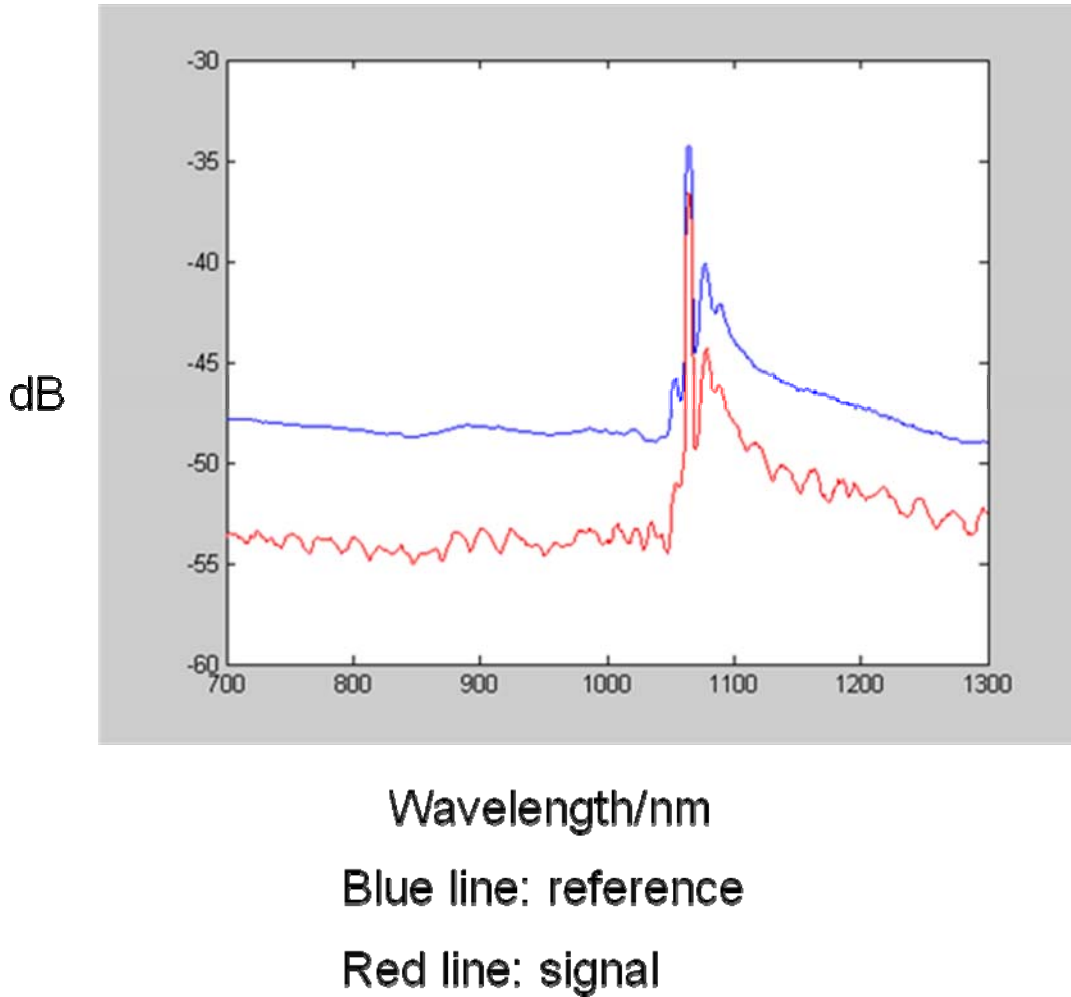


Figure 3-15: Total loss of sample 10

In addition, under optimal fabrication condition, the loss increases with the number of film bilayers. Sample 10 gives a very good example of this point. (See figure 3-16) Since the SHG intensity increase linearly with the bilayer number, we must tradeoff between the low-loss and the high-SHG intensity. In current measurement, the samples are all with film that less than 10 bilayers.

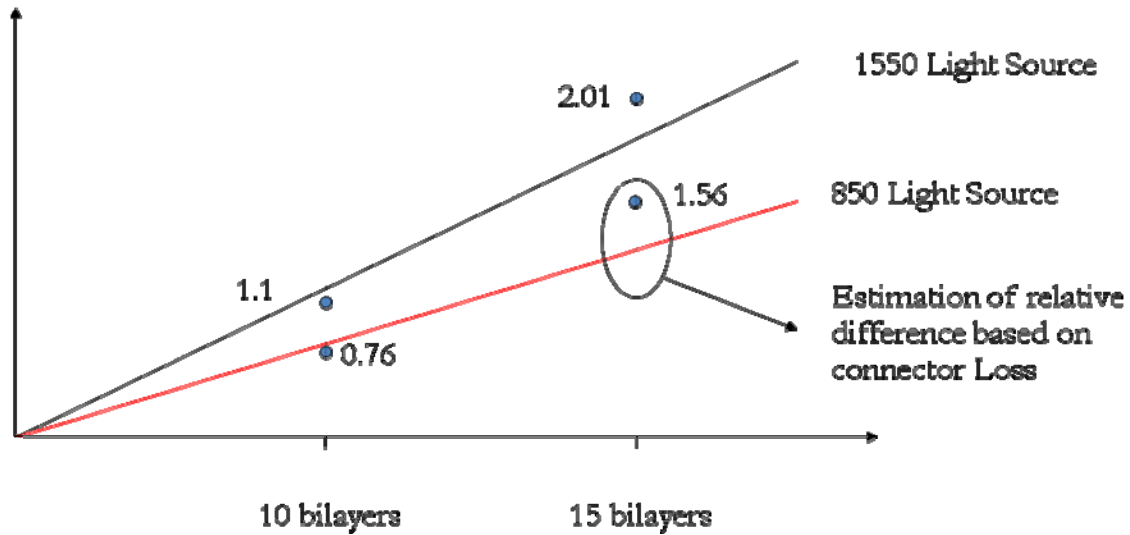


Figure 3-16: Analysis of the loss caused by film deposition for sample 10

All in all, by depositing films on selective fiber tapers, we are able to fabricate a taper fiber with 5 bilayers PAH/PR film that has a total loss around only 1 dB, for example, sample 39 and sample 40. Our work on reducing film loss makes the nonlinear fiber quite practical for the industry application. Furthermore, if we adopt the new technology to a programmable slide stainer, which is commercially available, we can realize the high-speed synthesis of identical films with high surface quality on multiple substrates while saving time and labor. Last but not least, our research on film surface improvement is a good reference for micro-scale characterization of other similar films.

chapter 4. Experiment Setup and Data Analysis

4.1 Experiment Setup and Measure Method

The setup for measuring the SHG fiber is shown in figure 4-1 as follows:

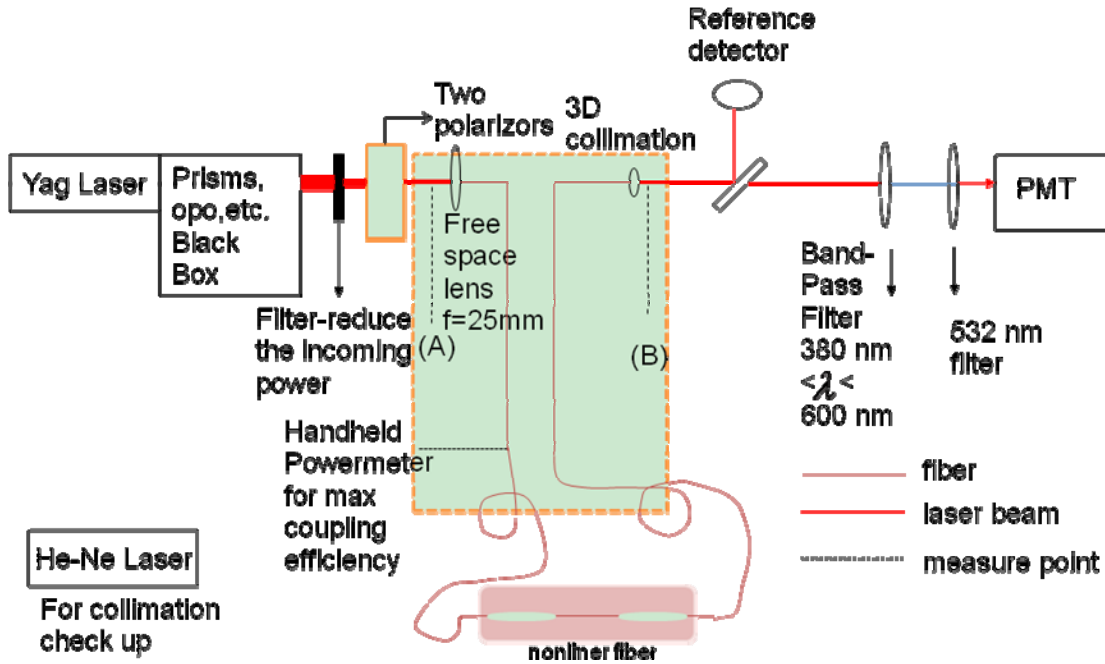


Figure 4-1: Figure 4-1: Setup for SHG measurement of nonlinear fiber sample

The beam comes out of a Q-switched Nd:YAG 10-Hz pulsed laser serves as a linearly polarized pump light with a wavelength of 1064 nm and a pulse energy of 450 mJ. An optical parametric oscillator (OPO) can be used to generate wavelengths other than 1064 nm. Some prisms are used to reflect part of the beam to the direction of optical fiber and to transmit the rest to a “black hole”, which absorbs all the power that comes into it. One or more energy attenuators are utilized to regulate the maximum energy incident upon the fiber. A pair of polarizers is used to align the polarization of the incoming beam and adjust the energy precisely at place A. The beam is focused by a free space lens to the tip of a fiber, which is directly spliced to the nonlinear fiber. Then, an

optical lens is used for collimation at place B. After the beam comes out of the collimation lens, about 8% of it is diverted via a microscope slide to a large area photodiode (PD) detector, which measures the reference signal intensity. A band-pass filter and a spike filter centered about the second harmonic frequency are used to make sure that all light except for the second harmonic light is eliminated. An RCA 8550 large-area photomultiplier tube (PMT) powered by a Bertran 230-03-R high voltage power supply operating at 1.8 kV collects the second harmonic light.

The following measurement steps are developed to produce accurate measure results while minimizing background noise:

1. Couple the beam from He-Ne laser into SMF28 and make sure collimated beam reflected into the reference detector and goes into the central of PMT

2. Measure SHG of SMF28 which is the same length of the sample

We connect a nonlinear fiber into the optical path by splicing the two ends of the sample to two connected fiber at points (1) and (2). See Figure 4-2 as follows:

3. Measure SHG of the sample which is made of SMF28

A single mode fiber can generates a small amount of SHG under high pump powe. We consider the SHG generated by a common single mode fiber as the background noise. After we measure SHG of a single mode fiber, we can compare the result with that of a nonlinear fiber. If we observe a significant larger SHG signal from the nonlinear fiber sample, we can conclude that the observed second harmonic signal is not due to the background noise but a result of the nonlinear structure that we proposed.

4. Couple the beam from He-Ne laser into SMF28 and check with the collimated beam to see whether it is still reflected into the reference detector and goes into the PMT

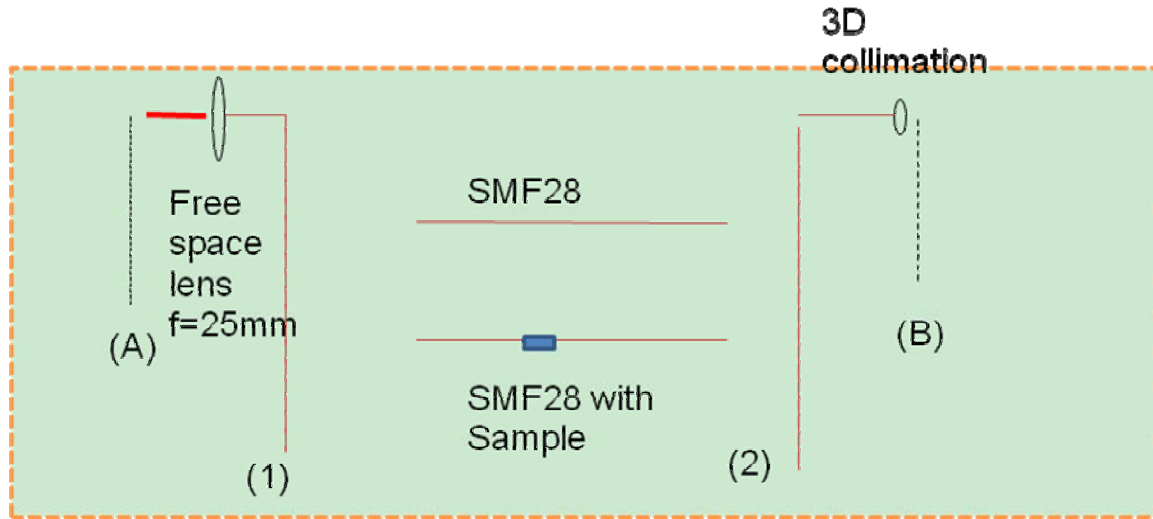


Figure 4-2: Measurement step 2 and 3

4.2 Data Analysis

4.2.1 Early SHG measurement of fiber taper with (PAH/PR)₅ film:

The early measurement results for single mode fiber SMF28 and sample (PAH/PR)₅ made of SMF28 show two linear relationships. (See figure 4-3) The first is the relationship between the reference signal and the power out of Collimation lens at B point. The second is the relationship of the reference signal and the square root of SHG. Different bare fibers have different ratios of the output out of Collimation lens to the reference signal because of the different length of bare fibers and different experiment errors. However, SHG from SMF28 is low and does not change much with different fibers (got verified when $B < 100\mu\text{W}$).

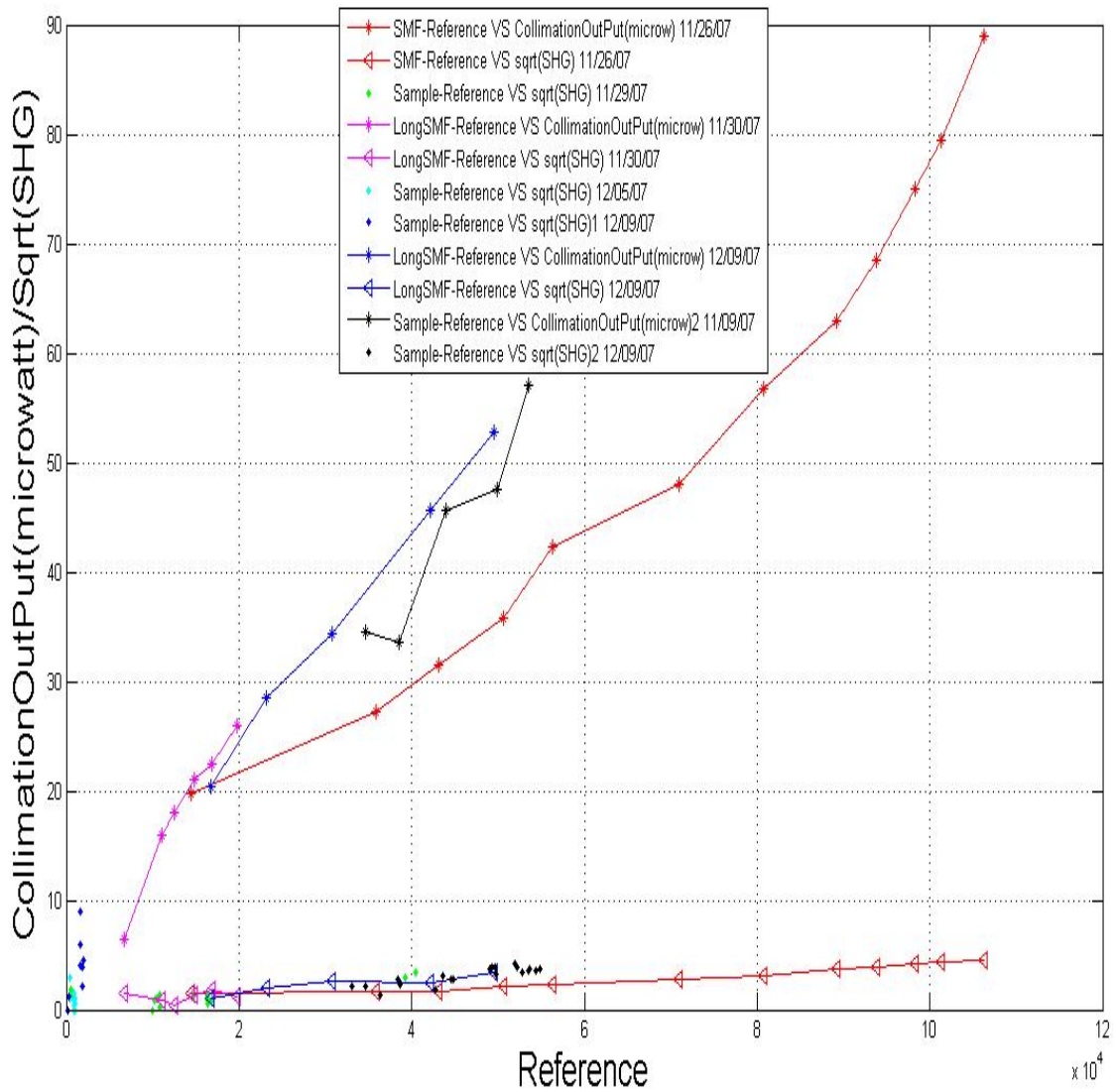


Figure 4-3: Early measurement of bare single mode fiber and fiber taper with nonlinear film

The observation of SMF28 provides us with a good knowledge of the background noise at different reference signals. In addition, at the condition that the excitation power is not high enough, we can see that the SHG signal of the nonlinear fiber is bigger than that of SMF28 .

4.2.2 Measurement of a fiber taper coated with (PAH/PB)₁₀ film:

The SHG coefficients of a fiber taper coated with (PAH/PB)₁₀ film with salt is much bigger than that of (PAH/PR)₅ (See section 3.2.3 for detail). Even at low excitation power, we are able to demonstrate the SHG difference between the nonlinear fiber and a single mode fiber. Figure 4-4 compares the SHG comes out of sample 48 and that out of SMF28 with the same length. Each reference and SHG intensity of SMF28 is averaged among at least 500 pulses and that of sample are averaged among 50 pulses. Even though not as stable as that of SMF28, the SHG efficiency of sample 48 is large enough to exceed the background noise and increase with the excitation power.

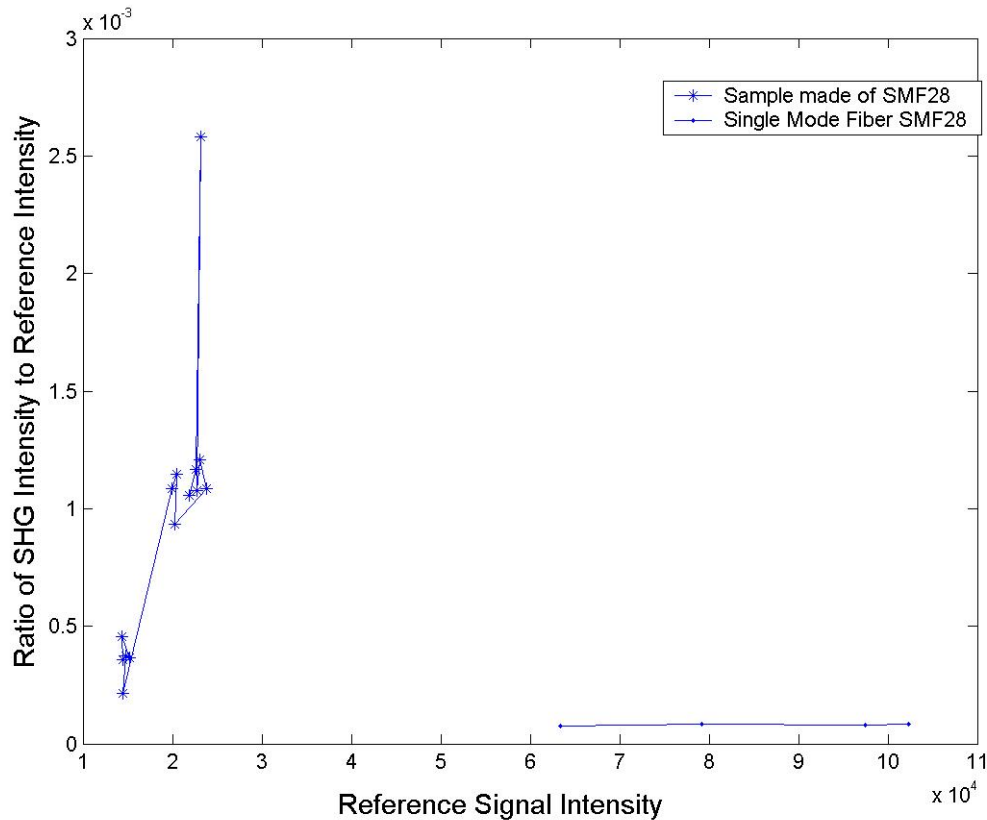


Figure 4-4: Compare of ratios of SHG to reference signal of the sample 48 and a single mode fiber with same length

4.2.3 The Impact of High Power at Forepart of SMF28

Nonlinear fiber sample, which normally has a higher loss than that of SMF28, may require a higher power at place A to have the same excitation power. This brings a

problem, how much is the SHG signal that comes out of the forepart of a fiber, which has a bigger excitation power? In order to solve this problem, the following experiment is designed as shown in Figure 4-5. The length of the forepart of the fiber is around 67.5 cm and we will find out the SHG signal when there is a SMF28 having the same loss (loop the fiber to produce the loss) and output power as that of the sample. Length estimated are subject to change with measurement (Each cleave may reduce the fiber length for less than 0.5cm).

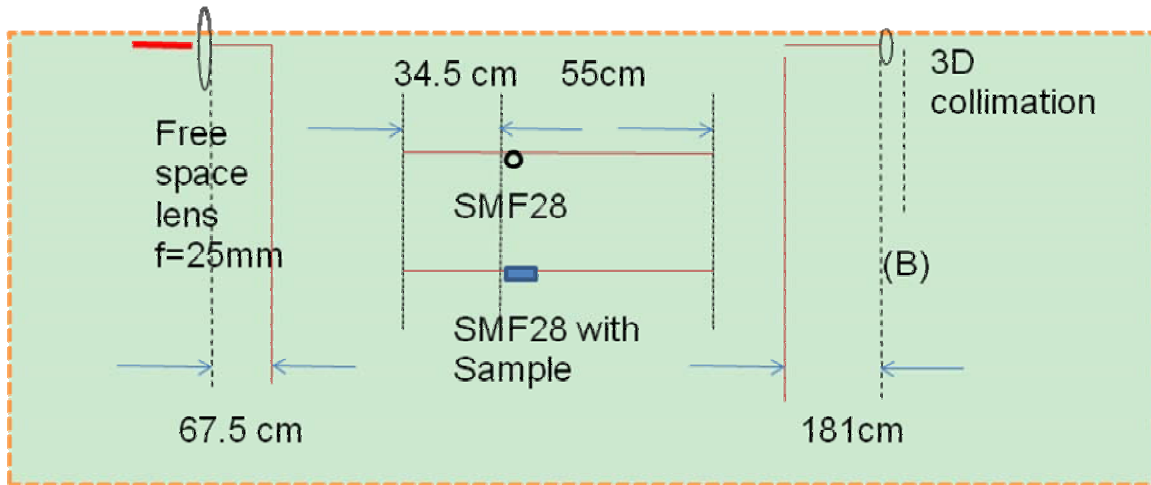


Figure 4-5: Experiments to explore the SHG comes out of the forepart of the fiber with high excitation power

Measure steps are as follows:

1. Measure the SHG of the fiber which is the same length of Sample 48 at high incoming power and maximum coupling efficiency;
2. Loop the fiber at the same position of the sample so that the collimation output at B is the same as that of the sample, which is caused by the high loss of the taper with film.
3. Measure the SHG of the looped fiber
4. Unloose the fiber to see whether the collimation output is the same before the loop

The result of this experiment is described by table 4-1 and illustrates that the high power launched at the forepart of the fiber will not produce the SHG signal that high enough to compare with that from the sample, because of the high loss of the SMF28/sample.

A(mW)	B(μ W)		Filter		Reference*Filter coefficient (AVG) (Reference Signal intensity)	SHG (AVG)
	Before measure	After measure	Ref	PMT		
3.09	147	139	20+40+80	no	164155.6	40.464
3.14	120 (no loop)	15	20+40+80	no	17252.9	9.04
	18	112 (no loop)				

Table 4-1: SHG of a SMF28 without loss and with high loss

Furthermore, we compare the SHG intensity of the looped SMF28 at 3.14 incoming power (the power at point A) with that of the sample 48 at 2.82 incoming power. Both collimation output is around 17 μ W, while the SHG intensities are different :(see table 4-2 for detail)

A(mW)	B(μ W)	Reference intensity	Signal	SHG Signal intensity
Sample 48				
2.82	17.5	19952.3		21.68
		20524.6		23.56
		20289.5		18.92
Looped SMF28				
3.14	16.5	17252.9		9.04

Table 4-2: SHG of sample 48 Vs SHG of looped SMF 28

It is clear that, though high power at forepart of fiber may produce some extra SHG signal, the noise is not as high as the sample production.

In this chapter, we have shown that by depositing (PAH/PB)₁₀ films around a fiber taper with a diameter around 5 μ m, we can obtain high SHG signal. The ratio of the obtained SHG signal to the excitation power for such a nonlinear fiber is more than 10 times of that of a 125 μ m single mode fiber with the same length.(see figure 4-4)

Furthermore, figure 3-8 has shown that different CHISAM films produce different SHG signals. SHG signal depends on both the number of the bilayers and the CHISAM molecules. This point is also proved in this chapter. Our experiment also indicates that a higher power at the forepart of a single mode fiber does not affect the SHG signal fundamentally. It is to say, even though a nonlinear fiber requires more incoming power than a common single mode fiber to generate the same excitation power, it is the nonlinear film, rather than the incoming power difference that results in the big SHG differences.

chapter 5. Conclusion and Future Work

5.1 Conclusion

In this thesis, we performed a theoretical analysis of silica-based nonlinear optical fiber and described how to characterize and experimentally implement the SHG measurement of such nonlinear fiber. According to our theoretical derivation, we find that a small radius and a long length of a nonlinear fiber with thick nonlinear film will help to result in a much high SHG efficiency. In order to verify our proposal, we fabricate taper fiber with radius less than 10 μm and deposit ISAM / CHISAM film around the taper part. Furthermore, we improve the taper setup and the film deposition method to reduce both the taper loss and the loss caused by film deposition.

We build a set of SHG measurement stage for the fiber sample and develop the measurement method during the measure experiments. According to our measurements, a nonlinear we fabricated by depositing CHISAM film around a fiber taper has a SHG efficiency that is more than 10 times higher than that of a common single mode fiber.(see figure 4-4)Thus, we provide strong evidence that centrosymmetric material can be used as SHG material.

5.2 Future work

At the present time, the SHG is far less than 10% because of the low excited power and the phase mismatch between the fundamental pump beam and second harmonic signal. In order to increase the SHG efficiency and make the nonlinear fiber more helpful in the nonlinear optics, we need to work toward two directions.

The first one is to increase the excitation power and, more specifically, the peak power. In order to do so, we need to improve the measurement setup to make it stable under a high incoming power. Our main difficulty in increasing the excitation power is that when coupling a high peak power into a section of fiber, the high-energy beam damages the tip of a silica fiber. See figure 5-1 for a damaged fiber tip.

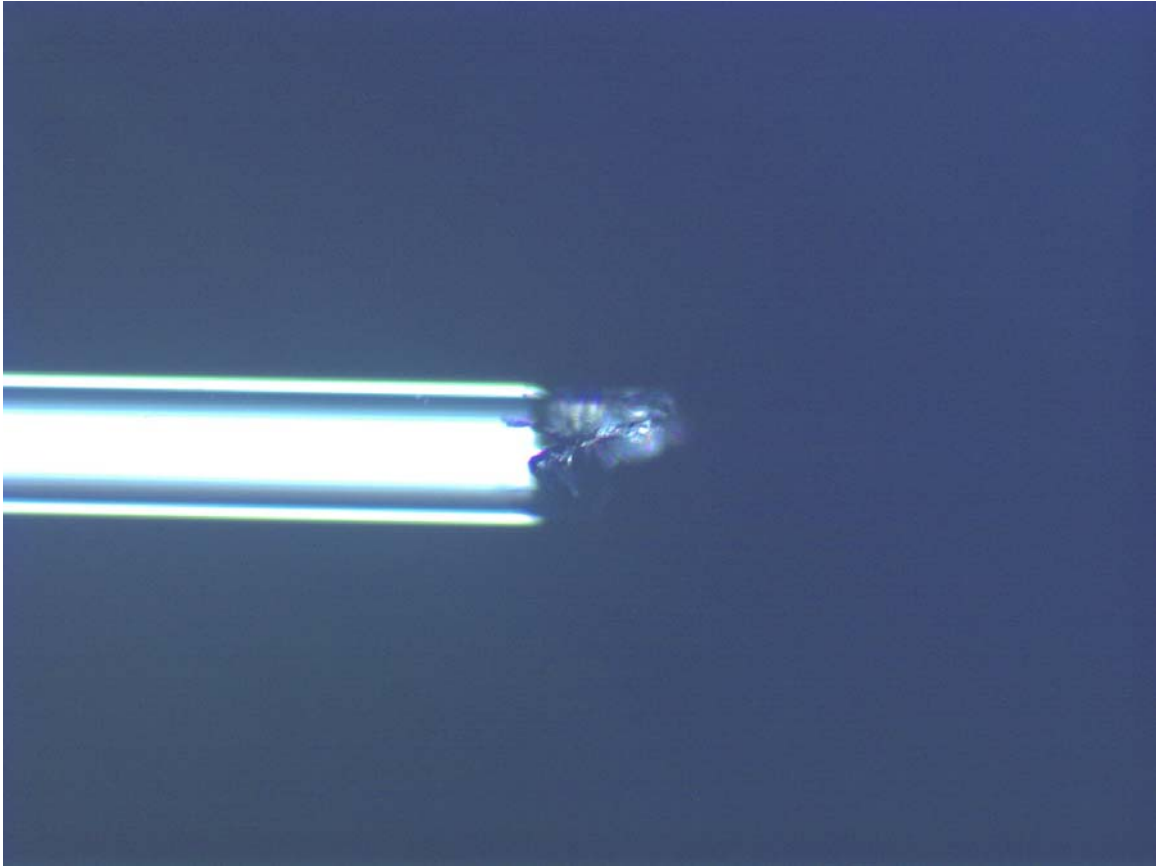


Figure 5-1: Experiments to explore the SHG comes out of the forepart of the fiber

The damage of fiber tip by the high pump power reduces the coupling efficiency dramatically. In order to connect a nonlinear fiber into the optical path, we fuse two ends of the fiber into the path rather than connect them with two FC/FC connectors. It is because that a high peak power will not damage the fiber tip seriously as long as it is fused together. As for the two ends of the optical path, which we make use of for launching power and exporting power, we have no ideal method to protect them from being sputtering by high power. Recently, we find out that, after it being exposed to a high power for some time, a section of silica fiber is not easy to be sputtered away, if we cleave away the surface of the fiber. We can make use of such fiber to protect the two ends of the optical path by fusing them together. This method, which helps our optical path stable under an exciting power as high as 10 mW, has a problem. After being exposed to a high excitation power for some time, the silica fiber generates a much higher

SHG signal. The SHG signal also increases with the power and the exposing time. Such a background noise would be a big issue if we want to explore the SHG difference between a nonlinear fiber and a single mode fiber at a high excitation power.

The other one is to satisfy the phase matching condition. We will tune the OPO to generate beams with varying wavelengths to determinate the influence of phase matching condition on SHG signals.

In addition, we will fabricate more nonlinear fibers with a broad diameter expand, different CHISAM/ISAM films, different number of film bilayers, different deposition conditions and different parameters. By comparing SHG efficiency of different nonlinear fibers, we will have an idea of what factors may affect the SHG efficiency.

Furthermore, we will work on theoretical analysis and simulation to establish a more complete theoretical model to understand the experimental result. We will also investigate other second order nonlinear processes, including parametric down conversion and sum frequency generation.

Last but not least, there is still a lot of work to do on loss reduction for thick films, such as $(\text{PAH/PB})_n$, where n is more than 20. The salt which increases the SHG susceptibility also increase the film surface roughness. For example, we may try spin coating assisted self assembly technique to reduce the loss of film with salt.

Reference

-
- [1] G. P. Agrawal, *Nonlinear Fiber Optics* (Academic Press, 2001).
- [2] U. Osterberg, W. Margulis, "Dye laser pumped by Nd:YAG laser pulses frequency doubled in a glass optical fiber" *Opt. Lett.* 11, 516-518 (1986).
- [3] R. A. Myers, N. Mukherjee, S. R. Brueck, "Large second-order nonlinearity in poled fused silica" *Opt. Lett.* 16, 1732-1734 (1991).
- [4] T. Fujiwara, M. Takahashi, A. J. Ikushima, "Second-harmonic generation in germanosilicate glass poled with ArF laser irradiation" *Appl. Phys. Lett.* 71, 1032-1034 (1997).
- [5] B. P. Antonyuk, N. N. Novikova, N. V. Didenko, O. A. Aktsipetrov, "All optical poling and second harmonic generation in glasses: theory and experiment" *Phys. Lett. A* 287, 161-168 (2001).
- [6] A. L. Moura, M. T. de Araujo, M. V. D. Vermelho, J. S. Aitchison, "Improved stability of the induced second-order nonlinearity in soft glass by thermal poling" *J. Appl. Phys.* 100, Art.033509 (2006).
- [7] G. Bonfrate, V. Pruneri, P. G. Kazansky, P. Tapster, J. G. Rarity, "Parametric fluorescence in periodically poled silica fibers" *Appl. Phys. Lett.* 75, 2356-2358 (1999).
- [8] W. Xu, P. Blazkiewicz, S. Fleming, "Silica fiber poling technology", *Adv. Mater.* 13, 1014-1018 (2001).
- [9] H. An, S. Fleming, "Hindering effect of the core-cladding interface on the progression of the second-order nonlinearity in thermally poled optical fibers" *Appl. Phys. Lett.* 87, Art. 101108 (2005).
- [10] A. Yariv, *Optical Electronics in Modern Communications* (Oxford U. Press, New York, 1997).
- [11] K. D. Singer, J. E. Sohn, and S. J. Lalama, *Appl. Phys. Lett.* 49, 248 (1986).
- [12] D. Jungbauer, B. Reck, R. Twieg, D. Y. Yoon, C. G. Wilson, and J. D. Swalen, *Appl. Phys. Lett.* 56, 2610 (1990).
- [13] J. W. Wu, J. F. Valley, S. Ermer, E. S. Binkley, J. T. Kenney, G. F. Lipscomb, and R.

-
- Lytel, *Appl. Phys. Lett.* 58, (225 ~1991).
- [14] I. R. Girling, N. A. Cade, P. V. Kolinsky, R. J. Jones, I. R. Peterson, M. M. Ahmad, D.B. Neal, M. C. Petty, G. G. Roberts, and W. J. Feast, *J. Opt. Soc. Am. B* 4, 950 (1987).
- [15] G. J. Ashwell, P. D. Jackson, and W. A. Crossland, *Nature (London)* 368, 438 (1994).
- [16] H. E. Katz, G. Scheller, T. M. Putvinski, M. L. Schilling, W. L. Wilson, and C. E. D. Chidsey, *Science* 254, 1485 (1991).
- [17] S. J. Yitzchaik, S. B. Roscoe, A. K. Kakkar, D. S. Allan, T. J. Marks, Z. Xu, T. Zhang, W. Lin, and G. K. Wong, *J. Phys. Chem.* 97, 6958 (1993).
- [18] K. B. Blodgett, *J. Am. Chem. Soc.* 56, 495 (1934).
- [19] L. Netzer and J. Sagiv, *J. Am. Chem. Soc.* 105, 674 (1983).
- [20] G. Cao, H.-G. Hong, T. E. Mallouk, *Acc. Chem. Res.* 25, 420 (1992)
- [21] G. Decher and J.-D. Hong, *Makromol. Chem. Macromol. Symp.* 46, 321 (1991).
- [22] G. Decher, J. D. Hong, and J. Schmitt, *Thin Solid Films* 210/211, 831 (1992).
- [23] Gero Decher, et al., *Science* 277, 1232 (1997).
- [24] C. Figura, et al., *Proceedings of SPIE, the international society for optical engineering*, p214, (2000)
- [25] Z. Wang, J. R. Heflin, R. H. Stolen, S. Ramachandran, *Appl. Phys. Lett.* 86, 223104 (2005)
- [26] R. Advincula, E. Aust, W. Meyer, W. Knoll, *ibid.*, p.3536.
- [27] J. J. Ramsden, Y. M. Lvov, G. Decher, *Thin Solid Films* 254, 246 (1995).
- [28] R. G. Freeman et al., *Science* 267, 1629 (1995).
- [29] J. Schmitt et al., *Adv. Mater.* 9, 61 (1997).
- [30] S. E. Yancey et al. *Journal of Applied Physics* 99, 034313(2006)
- [31] A. Laschewsky, *Eur. Chem. Chron.* 2, 13 (1997).
- [32] Y. M. Lvov and G. Decher, *Crystallogr. Rep.* 39, 628 (1994).
- [33] N. G. Hoogeveen, M. A. C. Stuart, G. Fleer, M. R. Bo¨ hmer, *Langmuir* 12, 3675 (1996).
- [34] R. Advincula, E. Aust, W. Meyer, W. Knoll, *ibid.*, p. 3536.
- [35] D. Laurent and J. B. Schlenoff, *ibid.* 13, 1552 (1997).

-
- [36] James R. Heflin, et. al, *Langmuir* 22, 5723-5727 (2006).
- [37] D. J. Markos, et. al, "Controlled core removal from a D-shaped optical fiber," *Appl. Opt.*, vol. 42, 7121-7125 (2003).
- [38] Shicheng Xue, et. al, *JOURNAL OF LIGHTWAVE TECHNOLOGY*, 25, 5 (2007)
- [39] Patrick J. Neyman, Second-Order Nonlinear Optical Characteristics of Nanoscale Self-Assembled Multilayer Organic Films, Ph.D. dissertation in Macromolecular Science and Engineering, Virginia Tech, Blacksburg, Virginia, June, 2004.
- [40] Yan Yin et. al., "Improvement on Surface Quality of Self-Assembly Films Deposited on Tiny or Un-Flat Surface", VTIP disclosure 08-046